BNL-228001-2025-JAAM

Au assisted smooth ultrathin epitaxial ZnO film grown by pulsed laser deposition on sapphire(0001)

X. Chen, L. R. Zhang

To be published in "Applied Surface Science"

February 2025

Center for Functional Nanomaterials

Brookhaven National Laboratory

U.S. Department of Energy

USDOE Office of Science (SC), Basic Energy Sciences (BES). Scientific User Facilities (SUF)

DISCLAIMER

Au assisted smooth ultrathin epitaxial ZnO film grown by pulsed laser deposition on sapphire(0001)

Xuegang Chen[1,2], Guoliang Wang[3], Jijie Huang[3], Xurong Qiao[4], Zhen Zhang[4], Tao Li[4], Lihua Zhang[5], Kim Kisslinger[5], Zonghuan Lu[6,7], Neha Dhull[6,7], Weichang Lin[6,7], Toh-Ming Lu[6,7], and Gwo-Ching Wang[6,7]

[1] Center of Free Electron Laser & High Magnetic Field, Institutes of Physical Science and Information Technology, Anhui University, Hefei 230601, China
[2] Information Materials and Intelligent Sensing Laboratory of Anhui Province, Anhui Key Laboratory of Magnetic Functional Materials and Devices, Anhui University, Hefei 230601, China
[3] School of Materials, Shenzhen Campus of Sun Yat-sen University, Shenzhen 518107, China
[4] State Key Laboratory for Mechanical Behavior of Materials, Department of Materials Science and Engineering, Xi'an Jiaotong University, Xi'an, Shaanxi 710049, China
[5]Brookhaven National Laboratory, Center for Functional Nanomaterials, P.O. Box 5000, Upton, New York 11973, USA
[6]Physics, Applied Physics and Astronomy Department, Rensselaer Polytechnic Institute, Troy, NY 12180, USA
[7]Center for Materials, Devices and Integrated Systems, Rensselaer Polytechnic Institute, Troy, NY 12180, USA

Corresponding authors: Gwo-Ching Wang wangg@rpi.edu; Xuegang Chen xgchen@ahu.edu.cn

Abstract
High quality ZnO has applications in photonics and electronics. Literature has shown that continuous, but rough ZnO film can be grown on sapphire substrate by pulsed laser deposition (PLD). In this work, ZnO and Au were co-deposited by PLD on sapphire(0001) substrates from a single ZnO target overlaid with an Au strip that serves as a catalyst. The reflection high-energy electron diffraction (RHEED) patterns show paired double spots from sample of ZnO-Au where the difference of in-plane lattice parameters between ZnO and Au is 11.4%. The two-dimensional (2D) reciprocal space maps constructed from azimuthal RHEED (ARHEED) patterns reveal parallel epitaxial relationship between ZnO and Au in the continuous ZnO-Au film on sapphire substrate. Transmission electron microscopy (TEM) cross section images and energy dispersive X-ray maps show minute Au nanocrystals distributed in the entire ultrathin ZnO film. Atomic force microscopy shows the root-mean-square roughness of the surface of ultrathin ZnO film with Au is in sub-nm range. The ARHEED and TEM results show that a couple of atomic percentages of Au co-deposited with ZnO catalyzes the growth of smooth ultrathin epitaxial ZnO film.

Key words
Pulsed laser deposition, ZnO, Au, sapphire, epitaxy, azimuthal RHEED, TEM

1. Introduction

ZnO is a direct bandgap semiconductor with 3.4 eV band gap in the near UV spectrum regime. It has been studied for over four decades. Its large exciton binding energy of ~60 meV allows excitonic emission to persist at room temperature. It also has high electron mobility and high thermal conductivity. Therefore, high quality bulk single crystal or thin films with minimal intrinsic defects and controlled incorporation of impurities have applications in photonics and electronics such as ultraviolet light emission devices [Janotti, Rep. Pro. Phys. 72, 2009]. Various methods have been used to grow high quality bulk ZnO single crystals. For epitaxial ZnO thin films it can be grown either homoepitaxially on bulk ZnO crystal substrate with zero lattice mismatch or heteroepitaxially with a lattice mismatch on substrates such as sapphire, GaN, and GaAs by pulse laser deposition (PLD) [Kumar 2014, J. nanosci and nanotech; Ohtomo 2005 Semicond Sci. Technol], chemical vapor deposition (CVD) [Ramos 2021, J. of Elec. Mater], metal-organic CVD [Pan 2006, J. of Crys. Growth], and molecular beam epitaxy (MBE) [Ozgur 2018, MBR chap 16]. For photonic and electronic applications, high quality single crystalline epitaxial ZnO films with minimal native defects and grain boundaries are required. Prior work of ZnO thin film deposited on sapphire(0001) by PLD shows a continuous film and the grain size in ZnO film has the (0001) orientation that increases as the growth temperature increases. However, the root mean square (RMS) roughness of the film is in the tens of nm or hundreds nm [Shan, J. Electroceramics, 2004].

Nanoscale Au particle is known as a catalyst in heterogeneous reaction [Sanchez 1999, J. Phys. Chem. A]. Nanoparticle Au has a relatively large number of corner and edge atoms that have low coordination numbers and the catalytic activity increases [Brodersen 2011, J. Catalysis; Hvolbæk 2007, Nanotoday]. A pre-deposited ultrathin Au layer was served as a catalyst in the PLD growth of ZnO in non-continuous films such as nanowires and nanosheets on c-sapphire surface [Weigand, J. of Cryst. Growth 2012]. These nanowires grew along the c-axis of ZnO but inclined ~37^{o} with respect to the surface normal direction. The (0001) plane of ZnO nanowires aligned with (10$\bar{1}$4) plane of c-sapphire. For ZnO nanosheets on c-sapphire, the nanosheets show no preferred orientation on sapphire and no epitaxial relationship could be unambiguously identified [Weigand, J. of Cryst. Growth 2012].

In this work, we report PLD of ultrathin continuous and smooth epitaxial films with sub-nm RMS on substrates sapphire (0001) from three kinds of single targets, ZnO, ZnO with a narrow Au strip that produces less amount of Au, and ZnO with a wide Au strip that produces a higher amount of Au. The films grown from these three kinds of targets are named samples P, L and M. The amounts of Au associated with samples L and M measured from X-ray energy dispersive spectroscopy (EDS) are 1.95% and 3.20% atomic percents, respectively. These samples were examined *ex situ* using azimuthal reflection high-energy electron diffraction (ARHEED) technique. Despite the 11.4% difference in the in-plane lattice parameters between Au and ZnO, the RHEED patterns and 2D maps constructed from ARHEED patterns show new findings. (1) RHEED patterns show paired doublet spots from ZnO and Au only at six major symmetric directions. The in-plane and out-of-plane lattice constants of these films are determined from paired doublet spots of ZnO and Au. (2) 2D maps show both ZnO(0001) and Au(111) are epitaxy with six-fold in-plane symmetry on sapphire substrates. The in-plane and out-of-plane epitaxial relationships of ZnO and Au are determined. (3) *Ex situ* TEM cross section images and EDS elemental maps show ZnO nanocrystals and Au nanocrystals co-exist and form a

continuous film. (4) Atomic force microscopy (AFM) images show the surfaces of these films are extremely smooth with RMS roughness less than 0.2 nm. The results from ARHEED, TEM and AFM support that Au serves not only as a catalyst to promote epitaxial growth of smooth epitaxial ZnO films but also forms epitaxial Au nanocrystals. This is quite different from previously observed ZnO nanowires or nanosheets using pre-deposited ultrathin Au layer on sapphire [Weigand, J. of Cryst. Growth2012].

2. Experimental

2.1 Growth of ZnO and Au on sapphire substrate

The pure ZnO film and ZnO films with two different amounts of Au were grown on Al_2O_3 (0001) substrates using pulsed laser deposition (PLD) method with a KrF excimer laser (Lambda Physik CompexPro 201, $\lambda = 248$ nm). Before a deposition, the base pressure of the chamber was pumped down to lower than 7.5×10^{-5} Pa or 5.6×10^{-7} Torr (1 Pa = 0.0075 Torr). Three separate targets (1) 1-inch diameter ZnO target, (2) an Au strip with 1.5 mm width and 1-inch length attached on the surface of 1-inch diameter ZnO target by the Ag paste, and (3) an Au strip with 3.0 mm width and 1-inch length attached on the 1-inch diameter ZnO target by the Ag paste were used for the deposition of P (pure ZnO), L (less Au), and M (more Au) films, respectively [Huang 2021, Huang 2021]. The deposition parameters were: oxygen pressure of 2 Pa, deposition temperature of 650 °C, laser frequency of 5 Hz, laser energy density about 1.42 J/cm^{-2}, and 3000 laser pulses. After each deposition, the film was naturally cooled down to room temperature under an oxygen pressure of 2 Pa.

2.2 Characterization of structural and stoichiometry

2.2.1 X-ray diffraction

X-ray Diffraction (XRD) measurements were carried out by using a Bruker D8 ADVANCE diffractometer with Cu K_α X-ray ($\lambda = 1.5418$ Å) operating at 1600 W. Coupled $\theta - 2\theta$ scan in the range of 10° - 90° with 0.02° increment was utilized. The scan time per step was 0.1 s. XRD $\theta - 2\theta$ scans, rocking curves, and azimuthal Φ (phi) scans of a specific crystal orientation of samples were measured using a Cu Kα source ($\lambda = 1.54$ Å) in a 2nd Bruker D8-Discover system.

2.2.2 Electron backscatter diffraction and energy-dispersive X-ray spectroscopy

Electron backscatter diffraction (EBSD) system is equipped with a NordlysNano detector, Oxford Instruments, integrated with a Karl Zeiss Ultra 1540 EsB system. EBSD was used to characterize the crystallographic properties of samples P, L, and M. For EBSD measurements, a 10 kV electron beam was used to scan the surface areas with a working distance of 18 mm, and a scan step size of 500 nm. The normal of the samples was tilted 70° to the impinging electron beam. The crystallographic orientation data was collected using the Aztec EBSD data acquisition software and post analyzed using the HKL Channel 5 package from Oxford Instruments for crystallographic orientation mapping and pole figure/inverse pole figure (IPF) plotting.

Energy-dispersive X-ray spectroscopy (EDS) was used to evaluate elemental compositions of samples L and M. The experimental configuration and conditions used are the same as the EBSD characterization. The spectra were collected in the analytical mode for the whole scanning area

of 50 μm × 40 μm for sample P, of 58 μm × 43 μm for sample L, and 50 μm × 40 μm for sample M.

2.2.3 Atomic force microscopy

Surface morphology was acquired by tapping imaging mode using a commercial Scanning Probe Microscopy system (MFP-3D, Oxford Instruments, USA). A clean and flat surface area at the central region of the sample was selected for 5 × 5 μm^2 and 2 × 2 μm^2 imaging. During the imaging process, a sharp silicon tip with a 7 nm nominal radius (AC160TS-R3, Olympus) is driven by a piezoelectric actuator that oscillates at the resonance frequency around 290 kHz and intermittently contacts the sample surface to acquire the surface morphology. The scanning angle was set to 90° and the tip-sample interaction was kept at the repulsive regime range throughout the measurements.

2.2.4 Azimuthal reflection high energy electron diffraction

The azimuthal reflection high-energy electron diffraction (ARHEED) technique has been described elsewhere [Xiang 2016]. In brief, the RHEED chamber has a base pressure of 10^{-9} Torr. It is equipped with an electron gun (model RDA-003G), a phosphor screen mounted on a 6-inch CF flange, and a digital camera (Nikon D700) positioned outside the chamber facing the phosphor screen. The sample was mounted on a holder with the sample's azimuthal rotation controlled by an ultrahigh vacuum stepper motor mounted on the shaft of a manipulator having x, y, and z translational and 360° rotational degrees of freedom. The electron gun generates 20 keV electron beam and 45 μA emission current incident at a glancing angle of ~1° on the sample surface. During the measurement the pressure increases to a lower range of 10^{-8} Torr due to the outgas of electron gun. The RHEED pattern from a sample surface was projected on the phosphor screen and recorded by the digital camera. In order to capture the entire reciprocal space structure above the sample surface, the sample was rotated 360° in-plane azimuthally with a 1.8° step size increment in 200 steps. We named it azimuthal RHEED (ARHEED) and the corresponding 200 RHEED patterns were recorded at each incremental step by a digital camera. A 2D map of diffraction spots was constructed from these 200 patterns as functions of radially outward $|\mathbf{k}_{\parallel}|$ and in-plane azimuthal angle ϕ at a chosen momentum transfer perpendicular to the surface $\mathbf{k}_{\perp}$. ARHEED data were collected from each sample at least once and up to three times to check the reproducibility.

2.2.5 Scanning transmission electron microscopy and EDS

To gain further information on the structure and chemical state of the samples P, L, and M, cross-sections of the samples were measured using scanning transmission electron microscopy (STEM) combined with elemental mapping using cross-sectional EDS maps of Zn and Au. The TEM lamellae samples consisting of Pt and Cr coatings were prepared in a Thermo Fisher Scientific Helios G5 dual-beam Ga^+ FIB system employing the *in-situ* lift-out method, followed by progressively thinning the sample with progressively lowering the ion beam voltages until a ~50 nm thickness was achieved. TEM sample analysis was performed in a Thermo Fisher Scientific X-FEG Talos 200X TEM system equipped with a Super-X energy dispersive X-ray spectroscopy (EDS) detection system. The characterization was conducted at 200 keV.

3. Experimental Results

The results including bulk structure by XRD, the atomic percentage of Au by EDS, and surface morphology and roughness by AFM of samples P, L, and M are presented in sections 3.1, 3.2, and 3.3, respectively. We refer samples P, L, and M for a ZnO film on sapphire, a ZnO film with less amount of Au on sapphire, and a ZnO film with more amount of Au on sapphire, respectively. The surface structure sensitive AREED and 2D maps of samples P, L, and M are presented in section 3.4. The STEM images, high angle annular dark field (HAADF) images, and EDS maps of samples P, L, and M are presented in section 3.5.

3.1. X-ray diffraction θ *vs.* 2θ scans and rocking curves of samples

X-ray diffraction (XRD) θ *vs*. 2θ scans of three samples P, L, and M are presented in this section. The atomic percentages of Au in samples L and M determined form EDS will be presented in section 3.2. Sample P is shown in Fig. 1(a). Two peaks located at $2\theta = 34.46^{o}$ and 72.59^{o} are consistent with calculated ZnO 002 and ZnO 004 peaks at $2\theta = 34.40^{o}$ and 72.51^{o}, respectively, using the ZnO's bulk lattice parameters a = b = 3.2539 Å, c = 5.2098 Å, $\alpha = \beta = 90^{o}$, and $\gamma = 120^{o}$. The peak at $2\theta = 41.67^{o}$ is identified as the calculated Al_2O_3 006 at 41.68^{o}. The Al_2O_3' bulk lattice parameters a = b = 4.785 Å, c = 12.991 Å, $\alpha = \beta = 90^{o}$, and $\gamma = 120^{o}$ are used in the calculation.

XRD θ *vs*. 2θ scan of sample L is shown in Fig. 1(d). Two ZnO peaks at $2\theta = 34.56^{o}$ and 72.81^{o} are identified as ZnO 002 and ZnO 004, respectively. The additional peak at $2\theta = 37.54^{o}$ is identified as Au 111 peak if compared with calculated Au 111 at 38.19^{o} using face center cubic Au's bulk lattice parameters a = b = c = 4.078 Å and $\alpha = \beta = \gamma = 90^{o}$.

From the XRD θ *vs*. 2θ scan of sample M in Fig. 1(g), a curve similar to that obtained from sample L is observed except the ratio of Au 111 peak intensity to ZnO 002 peak intensity is ~20 which is higher than the intensity ratio of ~10 for sample L. We conclude from XRD θ *vs*. 2θ scans that the out-of-plane orientations for Al_2O_3, ZnO and Au are (0001), (0001) and (111), respectively.

The high-resolution θ *vs*. 2θ scans and rocking curves of Zn 002 peaks from samples P, L, and M are shown in Figs. 1(b), (e), (h) and Figs. 1(c), (f), (i), respectively. The full-width-at-half-maximum (FWHM) of high-resolution θ *vs*. 2θ scans and rocking curves of Zn 002 peaks are listed in Table 1. These XRD data support that the samples probed by X-ray probing depth are of high crystal quality.

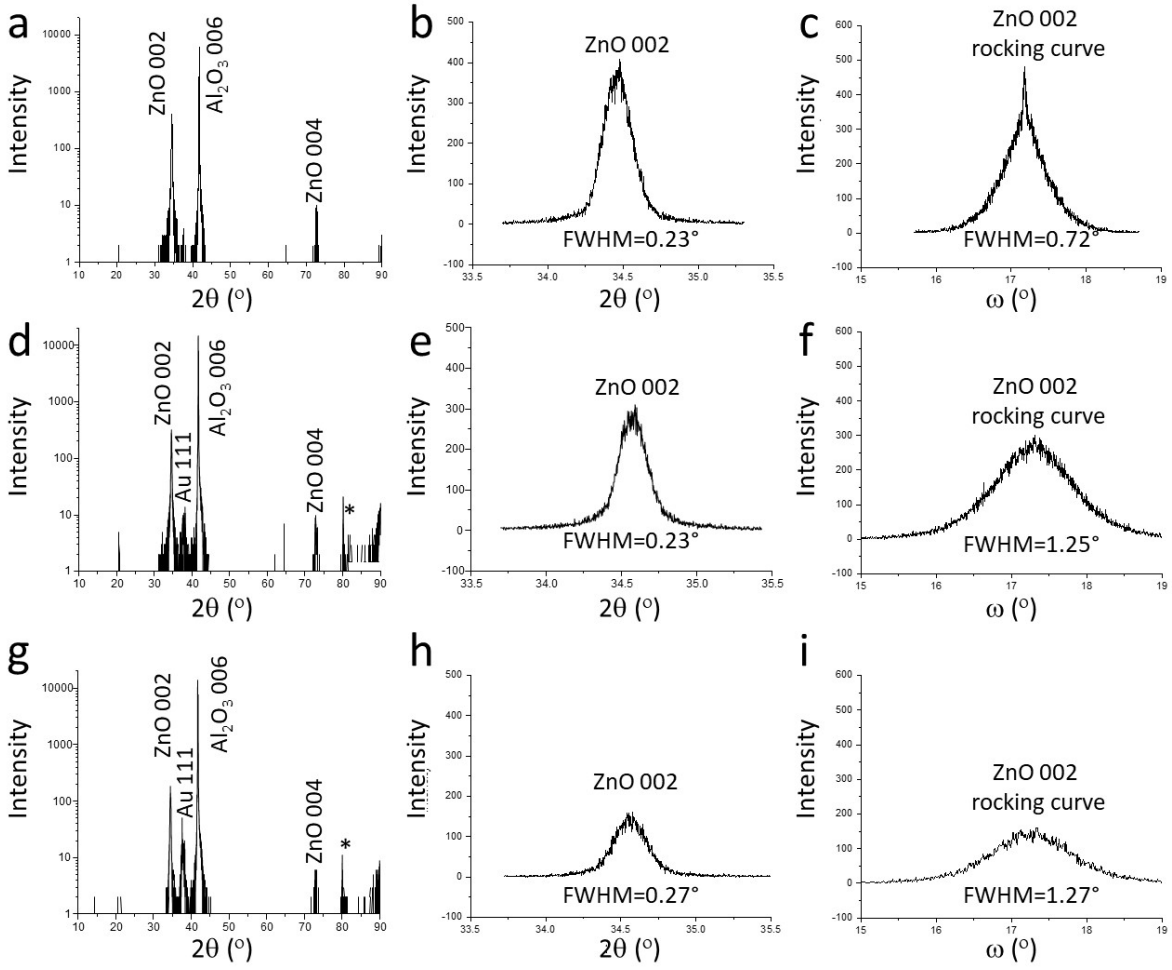

Fig. 1. X-ray diffraction data of ZnO samples. (a), (d), and (g) θ *vs*. 2θ scans of samples P, L and M, respectively. (b), (e) and (h), high-resolution θ *vs*. 2θ scans of ZnO 002 peak of samples P, L and M, respectively. (c), (f), and (i) rocking curves or intensity *vs*. ω scans of ZnO 002 peak of samples P, L and M, respectively.

Table 1 Results of X-ray diffraction of pulse laser deposited samples P (ZnO), L (ZnO with less Au), and M (ZnO with more Au). Substrates are sapphire(0001) for three ultrathin film samples.

Sample	XRD counts of ZnO 002 peak	FWHM (°) of ZnO 002 peak	FWHM (°) of rocking curve of ZnO 002 peak	Ave. FWHM (°) of 6 ZnO{11$\bar{2}$2} peaks in azimuthal direction	XRD counts of Au 111 peak	Ratio of XRD peak counts Au 111/ ZnO 002
P	400	0.23	0.72	1.72 ± 0.06	0	0
L	300	0.23	1.25	3.11 ± 0.37	~10	~1/30 = 0.03
M	200	0.27	1.27	3.41 ± 0.58	~20	~20/200 = 0.10

3.2 Energy dispersive x-ray spectroscopy of ZnO in sample P and Au atomic percentages in samples L and M

Energy dispersive x-ray spectroscopy (EDS) spectra of samples P, L, and M are shown in Figs. 2(a), (b) and (c), respectively. Peaks from Zn, O, Al, and C are observed in all three spectra. Note that the cps/eV numbers in the y-axis differ in three spectra. No Au peak is observed in sample P as expected. An Au peak is seen from sample L in Fig. 2(b) and a higher count of Au peak is seen from sample M in Fig. 2(c). The Au atomic percentages of samples L and M are estimated to be 1.95% and 3.20%, respectively.

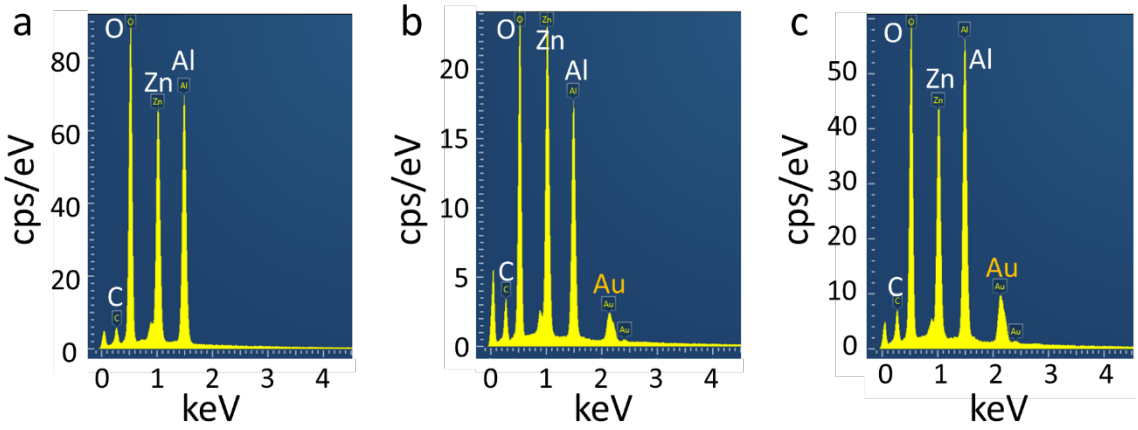

Fig. 2. Energy dispersive x-ray spectroscopy (EDS) spectra of (a) sample P, ZnO on sapphire, (b) sample L, ZnO with 1.95% Au on sapphire, and (c) sample M, ZnO with 3.20% Au on sapphire. Zn, O, Al, and C peaks are observed in all three spectra. The cps/eV in the vertical axis of (a), (b) and (c) varies in three spectra.

3.3 Atomic force microscopy images and surface smoothness of samples P, L, and M
Figures 3(a), (e), and (i) show 2 μm × 2 μm atomic force microscopy (AFM) images of samples P, L, and M, respectively. Figs. 3(b), (f), and (j) show the corresponding line scans of surface height in units of nm from Figs. 3(a), (e), and (i), respectively. Figs. 3(c), (g), and (k) show the corresponding surface height density distributions, respectively. Figs. 3(d), (h), and (l) show corresponding height-height correlation function (HHCF) [HN Yang book 1993], respectively.

The width for an arbitrary peak in the surface height line scan for sample L shown in Fig. 3(f) is similar to that of sample P in Fig. 3(b) but the width of a peak in the surface height line scan for sample M shown in Fig. 3(j) is wider than that of sample P shown in Fig. 3(b). Also, there are more small peaks within a wide peak for sample M than samples L and P. This qualitatively agrees with the visual inspection of protrusion sizes in the AFM images shown in Figs. 3(a), (e), and (i).

The variation of surface height in Figs. 3(c), (g), and (k) is between -0.6 nm to +0.6 nm. A small peak exists at ~0.55 nm that is close to the vertical lattice constant of ZnO. The root mean square (RMS) roughness values analyzed from AFM images of samples P, L, and M are 0.17 ± 0.01 nm, 0.19 ± 0.01 nm, and 0.17 ± 0.01 nm, respectively, very smooth.

Use the concept of HHCF from a self-affine surface, the lateral correlation lengths or "wavelengths" of surface height fluctuations in Figs. 3(b), (f), and (j) can be obtained [Zhao book 2001]. Figs. 3(d), (h), and (l) show plots of HHCF corresponding to AFM images in Figs. 3(a), (e), and (i), respectively. The lateral correlation length is extracted from the interception point of a horizontal red line parallel to the surface and a red slope parallel to the initial rise of HHCF [Lu et al, when interface gets rough 1995]. Project the interception points in Figs. 3(d), (h), and (l) on the x-axis as indicated by the vertical blue line, one obtains the lateral correlation length. The surface lateral correlation lengths are about 80, 50 and 100 nm for samples P, L, and M. These numbers are consistent with visual inspection of AFM images (Figs. 3(a), (e), and (i)) and surface height line scans Figs. 3(b), (f), and (j).

The lateral correlation length from ZnO with 3.20% Au is larger than that from ZnO with 1.95% Au. The lateral correlation length is approximately the lateral protrusion size. These sizes imply a higher amount of Au produces larger lateral feature size on surface than that of less Au.

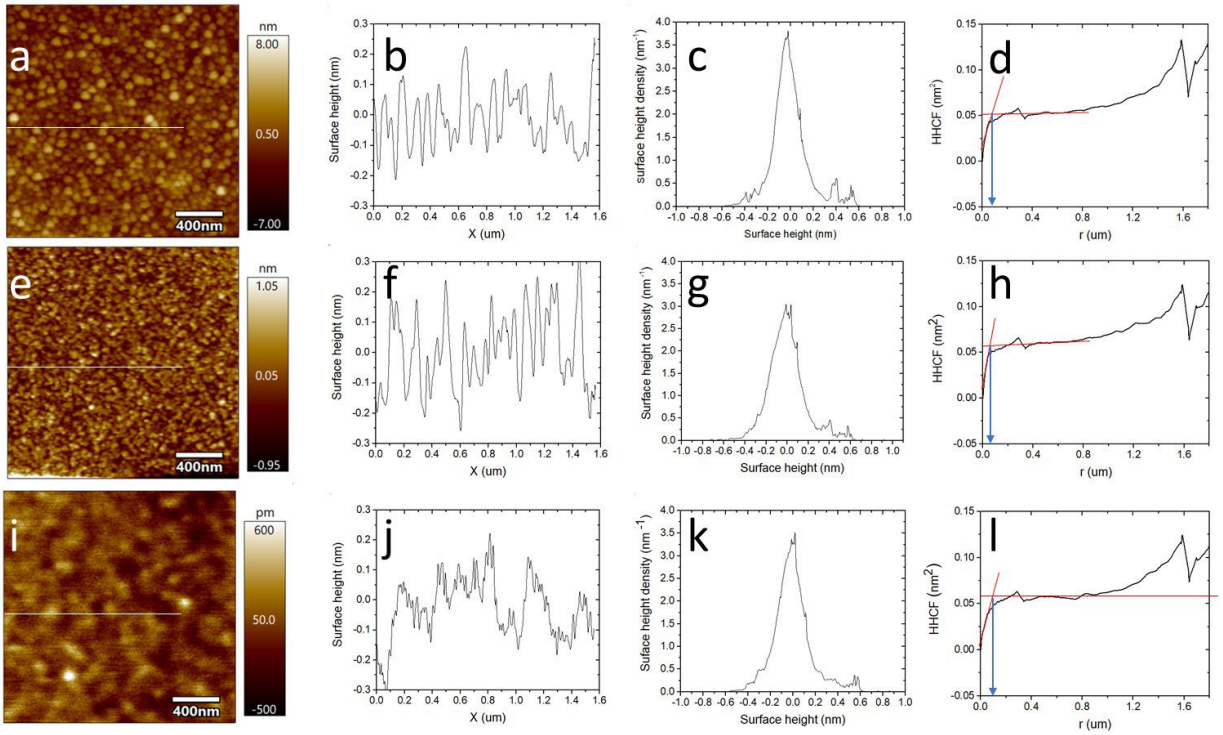

Fig. 3. (a), (e), (i) AFM images of ZnO, ZnO with 1.95% Au, and ZnO with 3.20% Au. All image sizes are 2 μm × 2 μm, (b), (f), (j) corresponding surface height line scans from white lines in (a), (e), (i) AFM images, respectively. (c), (g), (k) corresponding surface height densities, and (d), (h), (l) corresponding height-height correlation functions. The intersection of two red lines gives the lateral correlation length indicated by a blue arrow.

3.4 Reflection high-energy electron diffraction of samples P, L, and M

We will present RHEED patterns and a 2D map from sample P without Au as a reference in section 3.4.1 and follow by RHEED patterns and 2D maps of sample L (ZnO with 1.95% Au) in section 3.4.2 and sample M (ZnO with 3.20% Au) in section 3.4.3. The analysis method of lattice constants of ZnO from RHEED patterns and the symmetry of ZnO from 2D map are presented in section 3.4.1. For ZnO with 1.95% Au and ZnO with 3.20% Au, the analyses methods are similar to ZnO except additional stripes from Au in RHEED patterns appear and addition spots in 2D maps appear as paired doublet spots of Au and ZnO that allows us to determine the lattice constants of Au. The lattice constants of ZnO and Au determined in sections 3.4.2 and 3.4.3 are listed together with ZnO in **Table 2**.

3.4.1 Sample P

3.4.1.1 RHEED patterns and lattice parameters of ZnO from sample P

RHEED patterns at three azimuthal angles from sample P are shown in Figs. 4(a), 4(b), and 4(c). The absolute azimuthal angle depends on the initial sample mounting on the sample holder and the starting azimuthal angle for RHEED pattern collection is labeled as azimuth phi = 0°. Although the intensities of RHEED patterns are weak, spots and stripes are still visible. The spots and stripes indicate the transmission of electrons from surface protrusions with various finite sizes and the reflection of electrons from the smooth part of sample surface, respectively. The transmission spot is consistent with the particle like features in the AFM image shown in Fig. 3(a). Figs. 4(d) and 4(e) show integrated intensity profiles from the yellow boxes *vs*. parallel momentum transfer $\mathbf{k}_{\parallel}$ along two major symmetrical directions in Figs. 4(a) and 4(b), respectively. Where the $\mathbf{k}_{\parallel}$ is the momentum transfer parallel to the shadow edge. Single peaks in (00) and non-(00) stripes/spots are seen in Figs. 4(d) and 4(e). The average adjacent spacings $|\Delta\mathbf{k}_{\parallel}|$ in Figs. 4(d) and 4(e) are 2.37 ± 0.05 Å^{-1} and 4.04 ± 0.05 Å^{-1}, respectively. Convert these two measured reciprocal space spacing to real space in-plane lattice constant a in a hexagonal lattice through $\mathbf{G}(01) = 2\pi/d_{01}$ or $|\mathbf{a}|_{ZnO} = 2\pi/(|\Delta\mathbf{k}_{\parallel}|\sqrt{3}/2)$ and $\mathbf{G}(11) = 2\pi/d_{11}$ or $|\mathbf{a}|_{ZnO} = 2\pi/(|\Delta\mathbf{k}_{\parallel}|/2)$, one obtains a_{ZnO} = 3.06 ± 0.07 Å and 3.11 ± 0.05 Å, respectively. These lattice constants seem smaller than the ZnO bulk lattice constant a of 3.25 Å. It may be related to the lateral strain from the large lattice constant difference with the substrate sapphire' bulk lattice constant a = 4.78 Å.

To obtain the vertical lattice constant c, Fig. 4(f) shows integrated intensity from the yellow highlighted box *vs*. perpendicular momentum transfer $\mathbf{k}_{\perp}$ along the first stripe to the left of the 00 stripe in Fig. 4(c). Four peaks with approximately equal spacing are seen. The average adjacent $|\Delta\mathbf{k}_{\perp}|$ value is 1.25 ± 0.05 Å^{-1}. Through the reciprocal relationship $c = \frac{2\pi}{|\Delta\mathbf{k}_{\perp}|}$ one obtains c = 5.03 ± 0.20 Å, consistent with bulk lattice constant of 5.21 Å within the experimental uncertainty.

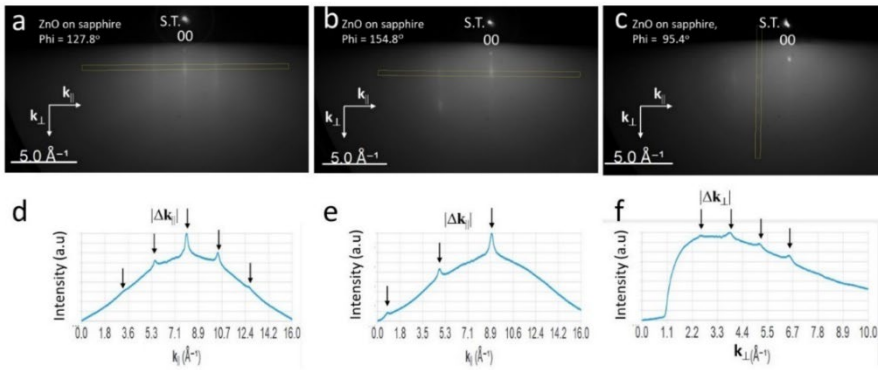

Fig. 4. Sample P (ZnO film on sapphire). RHEED patterns recorded at three azimuthal angles phi under 20 keV incident electron energy. (a) 127.8°, (b) 154.8°, and (c) 95.4°. The zone axes in (a), (b), and (c) are along $[01\bar{1}0]$, $[11\bar{2}0]$ and $[\bar{1}2\bar{1}0]$ directions, respectively. (d) and (e) integrated intensity *vs*. momentum transfer parallel to the surface $\mathbf{k}_{\parallel}$ from the yellow horizontal boxes in (a) and (b), respectively. (f) Integrated intensity *vs*. momentum transfer perpendicular to the surface $\mathbf{k}_{\perp}$ from the yellow vertical box along the first stripe to the left of 00 stripe/spots.

Table 2 Measured lattice parameters from RHEED patterns of samples P, L, and M along major symmetrical directions of ZnO(0001) and Au(111) as well as along the direction that is 30° azimuthal angle from the major symmetrical directions. Bulk lattice constant a of ZnO(0001) and nearest neighbor distance a_{nn} of Au(111) are listed in the 4th column. Bulk lattice constant c of ZnO(0001) and interlayer distance d_{111} of Au(111) are listed in the 7th column. Note the azimuthal angles phi $\phi = 0°$ and $\phi = 30°$ in the table corresponding to $<11\bar{2}0>$ directions and $<01\bar{1}0>$ directions (30° apart from $<11\bar{2}0>$ directions), respectively. Experimentally the measured average in-plane $\Delta k_{\parallel}$ ($Å^{-1}$) is from RHEED patterns along $<11\bar{2}0>$ and $<01\bar{1}0>$ directions. Data related to Au are in blue.

Sample			Measured in-plane $\Delta k_{\parallel}$ ($Å^{-1}$)	Measured lattice constant a for ZnO or d_{110} for Au (Å)	Bulk a for ZnO or d_{110} for Au (Å)	Measured out-of-plane $\Delta k_{\perp}$ ($Å^{-1}$)	Measured lattice constant c for ZnO or d_{111} for Au	Bulk c (Å) for ZnO or d_{111} for Au (Å)
P	ZnO	$\phi = 0°$ $\phi = 30°$	2.37 ± 0.05 4.04 ± 0.05	3.06 ± 0.07 3.11 ± 0.05	3.25*	1.25 ± 0.05	5.03 ± 0.20	5.20
L	Au	$\phi = 0°$ $\phi = 30°$	2.60 ± 0.05 4.51 ± 0.08	2.79 ± 0.05 2.78 ± 0.05	2.88**	2.60 ± 0.10	2.41 ± 0.10	2.35
	ZnO	$\phi = 0°$ $\phi = 30°$	2.29 ± 0.05 3.97 ± 0.08	3.17 ± 0.07 3.16 ± 0.07	3.25	1.21 ± 0.05	5.19 ± 0.25	5.20
M	Au	$\phi = 0°$ $\phi = 30°$	2.65 ± 0.05 4.50 ± 0.10	2.74 ± 0.05 2.79 ± 0.06	2.88	2.59 ± 0.10	2.42 ± 0.09	2.35
	ZnO	$\phi = 0°$ $\phi = 30°$	2.36 ± 0.05 4.00 ± 0.10	3.07 ± 0.07 3.14 ± 0.08	3.25	1.23 ± 0.04	5.11 ± 0.17	5.20

*Hexagon ZnO's bulk lattice parameters a = b = 3.2539 Å, c = 5.2098 Å.
**FCC Au's bulk lattice parameters a = b = c = 4.078 Å. The Au(111)'s nearest neighbor (nn) distance $a_{nn} = d_{110} = a/\sqrt{2} = 2.88$ Å and the interlayer spacing $d_{111} = c/\sqrt{3} = 2.35$ Å.

3.4.1.2 2D map of ZnO on sapphire(0001)

A 2D map of ZnO in reciprocal space was constructed from 200 RHEED patterns and shown in Fig. 5 for $\mathbf{k}_\perp = 3.67$ Å^{-1}. Maps at other $\mathbf{k}_\perp$ values are similar and not shown here. The reciprocal unit vectors **a*** and **b*** and the 1st, 2nd and 3rd order diffraction spots are visible. The symmetry of the lattice is hexagonal. Each spot on the map intercepts at a hexagonal lattice site using translational operations of unit vectors **a*** and **b*** except three spots labeled by one black arrow and two red arrows. All spots coincided on lattice sites are labeled as hk. In the supplementary document the X-ray diffraction in-plane azimuthal phi scans (Fig. S1) and EBSD pole figure (Fig. S2) support the 6-fold symmetry observed in the 2D map. The XRD in-plane azimuthal phi scan also shows that the ZnO lattice rotates 30° relative to that of sapphire(0001) lattice. A geometric superlattice area matching (GSAM) simulation in the supplementary document indicates that the ZnO lattice rotates 30° relative to that of sapphire(0001) lattice (Fig. S3) consistent with XRD azimuthal scan observation. The black arrow pointing spot is about halfway azimuthally between the first order diffraction spots or 30° from the major 6-fold symmetry direction. This could come from a secondary 30° in-plane rotational domain of ZnO relative to the primary ZnO domains. This weak spot implies that not all ZnO domains are rotated 30° relative to the sapphire substrate lattice. Each of the two red arrow pointing spots is about 10° away from major symmetry directions. This 10° rotation is also predicted in addition to 30° from GSAM simulations in the supplementary document (Fig. S3).

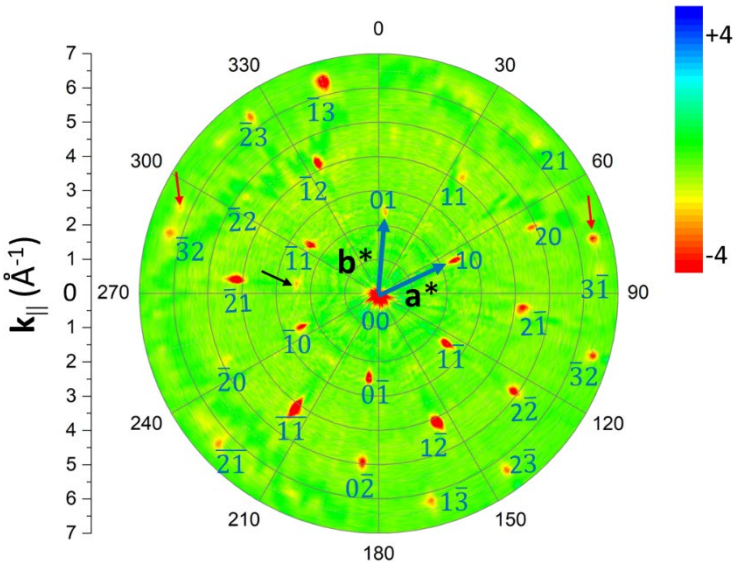

Fig. 5. A 2D reciprocal space map of ultrathin ZnO film on sapphire(0001) substrate sliced parallel to surface at vertical momentum transfer $\mathbf{k}_\perp = 3.67$ Å^{-1}. The **a*** and **b*** are reciprocal space unit vectors. Majority spots on hexagonal lattice sites are identified by hk from translational operations of **a*** and **b*** except one pointed by black arrow and two pointed by red arrows. These come from in-plane orientational domains deviated from major symmetrical directions.

3.4.2 Sample L (ZnO film with 1.95% Au on sapphire(0001))

In this section, we present RHEED patterns, in-plane and out-of-plane lattice parameters, and 2D map of sample L. Experimentally determined lattice constants are listed in Table 2. A new feature of sample L is Au stripes in RHEED patterns and Au spots in the 2D map.

3.4.2.1 Paired double peaks in RHEED patterns

Among the 200 collected RHEED patterns as a function of sample's in-plane azimuthal angle from sample L, two kinds of symmetric patterns with different lateral stripe spacing were observed. The patterns have stripes perpendicular to the shadow edge of the sample and elongated spots superpose on stripes. The pattern of the 1st kind in Fig. 6(a) at azimuthal angle ϕ = 351.2° repeats every 60° azimuthal angle. The zone axis is $[2\bar{1}\bar{1}0]$ or in one of six directions in the set of $<2\bar{1}\bar{1}0>$ directions. The pattern of the 2nd kind shown in Fig. 6(b) at ϕ = 21.6° is 30° azimuthal angle from the 1st kind. The zone axis is $[1\bar{1}00]$ or a direction in the set of 6 directions $<1\bar{1}00>$. The pattern of the 2nd kind in Fig. 6(b) also repeats every 60° azimuthal angle. Also, the intensity profiles corresponding to yellow boxes in the patterns in Figs. 6(a) and 6(b) are shown in Figs. 6(c) and 6(d), respectively. The horizontal separation distance $|\Delta\mathbf{k}_{||}|$ between adjacent spots/stripes labeled by black arrows of the 1st kind shown in Fig. 6(c) is smaller than that of the 2nd kind labelled by blue arrows shown in Fig. 6(d). Table 2 lists lattice parameters of ZnO and Au determined from measured $|\Delta\mathbf{k}_{||}|$. Next 2 sub-sections are detailed steps.

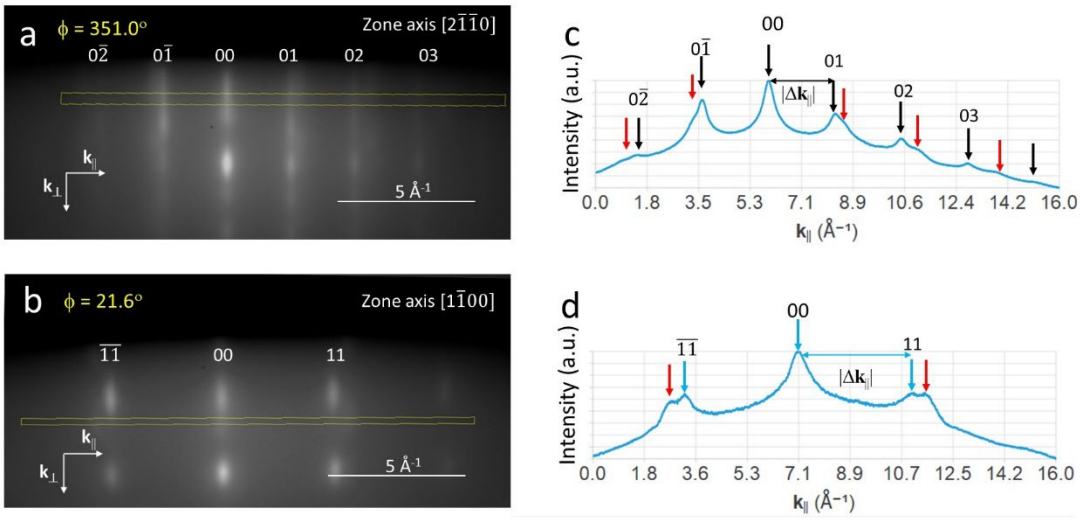

Fig. 6. RHEED pattern of sample L (ZnO with 1.95% Au). Zone axis along (a) the $[2\bar{1}\bar{1}0]$ direction, and (b) the $[1\bar{1}00]$ direction. (c) and (d) Integrated intensity *vs*. momentum transfer parallel to the surface $\mathbf{k}_{||}$ from the yellow horizontal boxes in (a) and (b), respectively. Intensity profiles show paired double peaks indicated by black and red arrows in (c) and blue and red arrows in (d).

3.4.2.1.1 In-plane lattice constants of ZnO(0001) and Au(111)

RHEED patterns from the 1st kind viewed from <$2\bar{1}\bar{1}0$> directions

The intensity profile *vs.* $\mathbf{k}_{\parallel}$ in Fig. 6(c) shows that besides primary peaks labeled in black color arrows, there are shoulders or weak peaks labeled in red color arrows near the black color arrows or pairs of double peaks. From XRD θ *vs*. 2θ scans, we learned that the surface orientations of ZnO and Au are ZnO(0001) and Au(111), respectively. The bulk lattice constant a_{ZnO} = 3.25 Å in the ZnO(0001) plane is larger than the nearest neighbor (nn) bulk distance $a_{Au,nn}$ = 2.88 Å in the Au(111) plane. It is expected that in the reciprocal space, the reciprocal space unit vectors $\mathbf{a}^*_{ZnO}$ < $\mathbf{a}^*_{Au,nn}$. The average reciprocal space separation $|\Delta\mathbf{k}_{\parallel}|$ between adjacent peaks labeled in black arrows in Fig. 6(c) is 2.29 ± 0.05 Å^{-1}. Assume $|\Delta\mathbf{k}_{\parallel}| = \mathbf{G}(01) = 2\pi/d_{01}$ where **G** and d_{01} are the reciprocal space vector and the real space interlayer spacing of 010 family planes of ZnO, respectively, and the $d_{01} = \sqrt{3}a/2$ from a hexagonal lattice, then the lattice constant $|\mathbf{a}|$ = a can be obtained from the measured $|\Delta\mathbf{k}_{\parallel}|$. Through the reciprocal relationship $\mathbf{G}(01) = 2\pi/d_{01}$ or $|\mathbf{a}|_{ZnO} = 2\pi/(|\Delta\mathbf{k}_{\parallel}|\sqrt{3}/2)$, one obtains a_{ZnO} = 3.17 ± 0.07 Å, close to the bulk ZnO lattice constant of 3.25 Å within the experimental uncertainty.

The average separation $|\Delta\mathbf{k}_{\parallel}|$ between adjacent peaks labeled in red arrows in Fig. 6(c) is 2.60 ± 0.05 Å^{-1}. Since this number is larger than 2.29 ± 0.05 Å^{-1} between adjacent black arrows, one can assume these red arrow pointing peaks are from Au(111). Similarly, one uses $|\mathbf{a}|_{Au,nn} = 2\pi/(|\Delta\mathbf{k}_{\parallel}|\sqrt{3}/2)$, one obtained $a_{Au,nn}$ = 2.79 ± 0.05 Å, slightly less than Au's nn distance of 2.88 Å. Note FCC(111) face of Au has a nn distance 2.88 Å and it is not the bulk lattice constant a of 4.08 Å. The average reciprocal space separation distance between adjacent pair of black and red arrows for the 01, 02, and 03 of paired double diffraction peaks in Fig. 6(c) are 0.30 ± 0.05 Å^{-1}, 0.59 ± 0.05 Å^{-1}, and 0.92 ± 0.10 Å^{-1}, respectively, an increasing trend in the reciprocal space separation as the order of diffraction increases. These data indicate that ZnO and Au are grown epitaxially on the sapphire substrate. This experimental trend of increasing spacing between adjacent pair of black and red arrows as the order of diffraction increases is expected and consistent with superlattice area matching simulations presented in section S.4 in the supplementary document.

RHEED patterns from the 2nd kind viewed from <$1\bar{1}00$> directions

The intensity profiles *vs.* $\mathbf{k}_{\parallel}$ in Fig. 6(d) show the average reciprocal space separation $|\Delta\mathbf{k}_{\parallel}|$ between adjacent peaks pointed by blue arrows is 3.97 ± 0.08 Å^{-1}. This reciprocal spacing along this direction is larger than that along the **G**(01) direction. We can assume this $|\Delta\mathbf{k}_{\parallel}| = \mathbf{G}(11) = 2\pi/d_{11}$ and $1/d_{11} = 2/a$ from a hexagonal lattice of ZnO. Then from the reciprocal relationship $|\mathbf{a}|_{ZnO} = 2\pi/(|\Delta\mathbf{k}_{\parallel}|/2)$, one obtained a_{ZnO} = 3.16 ± 0.07 Å, consistent with the value obtained from previous **G**(01) in Fig. 6(c) and close to the bulk ZnO lattice constant of 3.25 Å. The average separation $|\Delta\mathbf{k}_{\parallel}|$ between adjacent peaks labeled in red arrows in Fig. 6(d) is 4.51 ± 0.08 Å^{-1}. Similarly using inverse relationship between real and reciprocal space, one obtains $|\mathbf{a}|_{Au,nn} = 2\pi/(|\Delta\mathbf{k}_{\parallel}|/2)$ = 2.78 ± 0.05 Å. This value is slightly smaller than bulk Au's nearest neighbor distance, 2.88 Å. The average separation distance between a pair of blue and red arrows for the 1st order of paired diffraction peaks in Fig. 6(d) along **G**(11) is 0.54 ± 0.05 Å^{-1} that is ~1.8 times larger than the paired black and red arrowed peaks spacing of 0.30 ± 0.05 Å^{-1} in Fig. 6(c) along the **G**(01) direction. This is consistent with the theoretical ratio of $\mathbf{G}(11)/\mathbf{G}(01) = \sqrt{3} = 1.73$.

3.4.2.1.2 Out-of-plane lattice constants of ZnO(0001) and Au(111)

ZnO(0001) ~~Image 194~~

The out-of-plane lattice constant of an epitaxial film can be extracted from the intensity modulation along the momentum transfer perpendicular to the sample surface, $\mathbf{k}_\perp$. Figs. 7(a) and 7(a) show the same RHEED pattern of the 1st kind at $\phi = 349.2^o$, one of six major in-plane symmetric directions. The intensity profile from the straight through (S.T.) beam along the center 00 stripe in the $\mathbf{k}_\perp$ direction is shown in Fig. 7(c). There are four visible intensity bumps labeled by black arrows. Among the four bumps, two bumps near $\mathbf{k}_\perp = 5$ Å^{-1} are merged together. It is challenging to tell which bump is diffraction from ZnO and which is from Au. If the intensity profile *vs*. $\mathbf{k}_\perp$ is scanned from the non-00 stripe, then the lattice mismatch between ZnO and Au shows up as close but separated stripes at different $\mathbf{k}_\parallel$ values. The intensity profiles along the inner stripes of 01 or $0\bar{1}$ are from ZnO and the outer stripes are from Au. The intensity profile *vs*. $\mathbf{k}_\perp$ along the yellow line of the inner 01 spot/stripe to the right side of 00 stripe in Fig. 7(b) is shown in Fig. 7(d). Four visible bumps with almost equal $|\Delta\mathbf{k}_\perp|$ spacing are seen and labeled by blue arrows. The average $|\Delta\mathbf{k}_\perp|$ between adjacent two bumps are 1.21 ± 0.05 Å^{-1}. Through $2\pi/|\Delta\mathbf{k}_\perp|$, this 1.21 ± 0.05 Å^{-1}value converts to a real space interlayer spacing 5.19 ± 0.20 Å, close to ZnO's bulk lattice constant c of 5.20 Å. The intensity profile *vs*. $\mathbf{k}_\perp$ along the inner spot/stripe of $0\bar{1}$ to the left side of 00 stripe in Fig. 7(b) also gives a similar measured $|\Delta\mathbf{k}_\perp|$ value and the profile is not shown here.

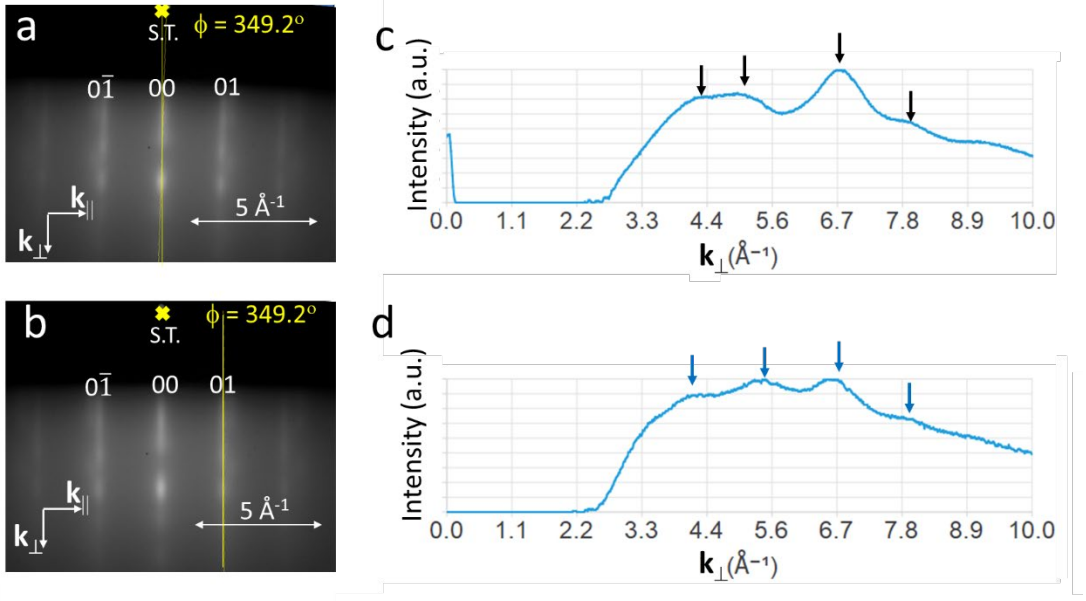

Fig. 7. (a) and (b) the same RHEED patterns of sample L (ZnO with 1.95% Au) viewed along the [2$\bar{1}\bar{1}$0] zone axis direction at $\phi = 349.2^o$. (c) and (d) Intensity *vs*. momentum transfer perpendicular to the surface $\mathbf{k}_\perp$ from the 00 stripe/spots and 01 stripe/spots along the yellow vertical line in (a) and (b), respectively.

Au(111) ~~Image 77~~

The intensity of outer spot/stripes of non-00 spot/stripes from Au are weak in the RHEED pattern at azimuthal angle ~~(Image 194)~~ ϕ = 349.2° in Fig. 7(a). For RHEED pattern of the 2nd kind (ϕ = 30°) at other major in-plane symmetrical directions such as at azimuthal angle ϕ = 138.6°, the intensity for outer spot/stripe from Au is stronger as seen in Fig. 8(a). The intensity profile from the straight through beam along the center 00 spot/stripe in the $\mathbf{k}_\perp$ direction is shown in Fig. 8(b). There are four visible bumps. Again, it is challenging to tell which bump is diffraction from ZnO and which is from Au. To the left of 00 spot/stripe in Fig. 8(a) there are two vertically separated spot/stripes visible under $\bar{1}2$ stripe. The inner one of $\bar{1}2$ closer to the 00 spot/stripe is from ZnO and the outer one is from Au because $\mathbf{a}^*_{ZnO} < \mathbf{a}^*_{Au,nn}$. The intensity profile *vs*. $\mathbf{k}_\perp$ along the vertical yellow line of the inner spot/stripe in Fig. 8(c) is shown in Fig. 8(d). Two visible bumps labeled by blue arrows are seen and aligned with two pumps labeled by blue arrows in Fig. 8(b). The intensity profile *vs*. $\mathbf{k}_\perp$ along the vertical yellow line of the outer spot/stripe in Fig. 8(e) is shown in Fig. 8(f). Two visible bumps labeled by red arrows align with two pumps labeled in red arrows in Fig. 8(b). The average $|\Delta\mathbf{k}_\perp|$ between two bumps labeled by red arrows is 2.6 ± 0.10 Å^{-1}. This converts to a real space interlayer spacing of 2.41 ± 0.10 Å, consistent with bulk Au(111)'s interlayer spacing of 2.35 Å. After the identification of ZnO and Au peaks from Figs. 8(d) and 8(f), One can go back in Fig. Fig. 8(b) to identify the red peaks are from Au and blue peaks are from ZnO.

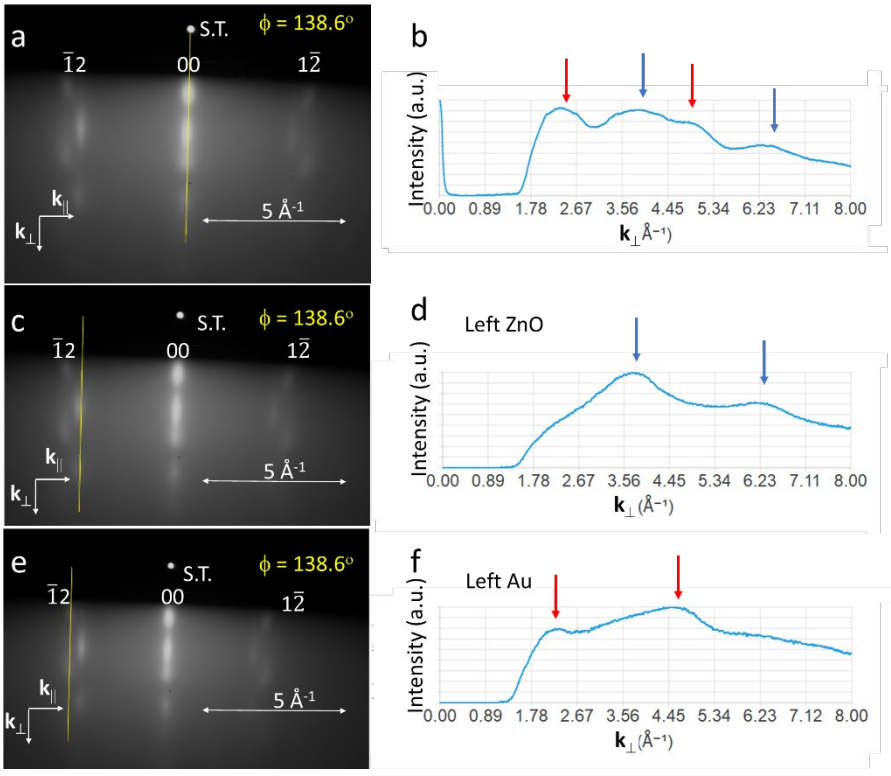

Fig. 8. (a), (c) and (e) are the same RHEED pattern of sample L (ZnO with 1.95% Au) viewed along the [$\bar{1}$100] zone axis direction. (b), (d), and (f) intensity *vs*. momentum transfer perpendicular to the surface $\mathbf{k}_\perp$ from the 00, inner $\bar{1}2$, and outer $\bar{1}2$ stripe/spots along the vertical yellow lines in (a), (c) and (e), respectively.

3.4.2.2 2D map reveals pairs of double spots from ZnO and Au

Figure 9 shows a 2D reciprocal space map of sample L constructed from 200 RHEED patterns. The 2D map presented is a cut parallel to the surface at the value of $|\mathbf{k}_\perp| = 3.87$ Å^{-1}. The 1st order diffraction spots {10} are located at $|\mathbf{k}_\parallel|$ distance 2.3 ± 0.05 Å^{-1} and the unit vectors **a*** and **b*** are labeled and the angle between them is 60°. The 2nd order diffraction spots {20} are located at $|\mathbf{k}_\parallel|$ distance 4.6 ± 0.08 Å^{-1} ($= 2 \times 2.3$ Å^{-1}). The {11} diffraction spots 30° azimuthal angle away from either {10} or {01} locate at 4.0 ± 0.08 Å^{-1}. Apply translational operations of unit vectors **a*** and **b***, all spots coincide with hexagonal lattice sites. The doublet spots circled by solid white ovals are seen at $2\bar{1}$, $1\bar{2}$, $\bar{1}\bar{1}$, $\bar{2}1$, and $\bar{1}2$ spots at azimuthal angles ϕ near 90°, 150°, 210°, 270°, 330°, about every 60° azimuthal angle apart. The exception is 11 spot near ϕ = 30°. The doublet spots from ZnO and Au should also be seen at the first order diffraction such as {10} but the intensity is weak and ZnO and Au spots are close and not obviously seen in a 2D map. But the paired double spots are seen in intensity profiles *vs.* $\mathbf{k}_\parallel$ in Figs. 6(b) and 6(d).

The spots closer to the center in the pair of double spots are from ZnO and the spots further away from the center in the pair of double spots are from Au. Despite some spots having weak intensity, the symmetry of spots is consistent with a 6-fold hexagonal lattice with the [0001] out-of-plane direction for ZnO and the [111] out-of-plane direction for Au. The 2D map of sample L reveals both Au(111) and ZnO(0001) are epitaxy with respect to the sapphire substrate. The two spots in each pair of double spots are radially parallel along 6 major symmetric directions despite a 11.4% theoretical lattice difference between ZnO lattice constant a of 3.25 Å and Au' nearest neighbor distance a_{nn} of 2.88 Å.

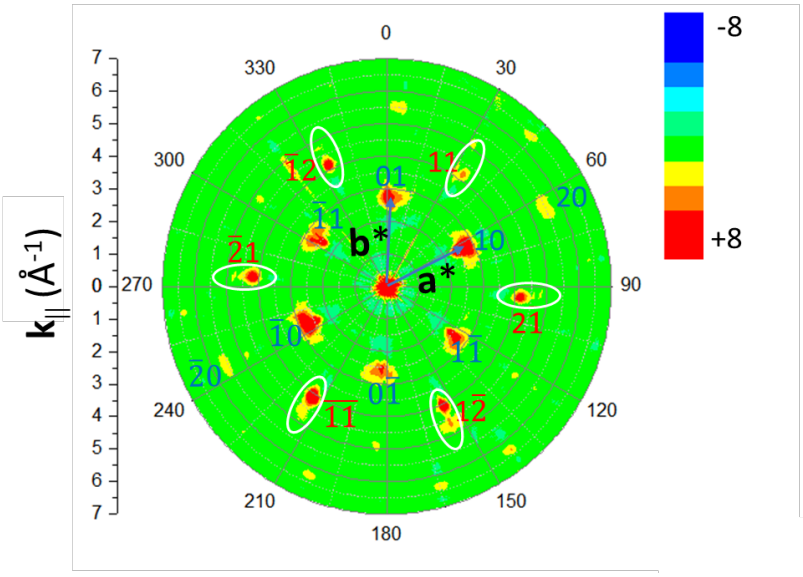

Fig. 9. A 2D reciprocal space map of sample L (ZnO with 1.95% Au) constructed from 200 azimuthal angle dependent RHEED patterns. **a*** and **b*** are reciprocal space unit vectors with 60° between them showing a six-fold symmetry. Doublet spots circled by white ovals from ZnO and Au exist along the six major symmetrical directions. The spot closer to the center in the pair of double spots is from ZnO and the spot further away from the center in the pair of double spots is from Au.

3.4.3 Sample M (ZnO with 3.20% Au on sapphire(0001))

This section presents RHEED patterns, in-plane and out-of-plane lattice parameters, and 2D map of sample M. Additional stripes and spots from Au are observed similar to that of sample L. However, the RHEED pattens are weaker and 2D map shows less quality as compared with that of sample L.

3.4.3.1 Paired double peaks in RHEED patterns and lattice constants of ZnO and Au

Table 2 lists lattice parameters of ZnO and Au measured from sample M. Next two sub-sections are details.

3.4.3.1.1 *In-plane lattice constant determined from* $\Delta\mathbf{k}_{\parallel}$

Figure 10(a) shows a RHEED pattern collected at azimuthal angle $\phi = 322.2^{o}$. In general, the intensity in all 200 patterns is weak but spots are visible in certain azimuthal angles. Fig. 10(b) shows intensity *vs*. momentum transfer parallel to the surface $\mathbf{k}_{\parallel}$ integrated from the horizontal yellow box in Fig. 10(a). Paired double weak spots are labeled by red and blue arrows on peak $0\bar{1}$ and peak 01. The average reciprocal space distance from 00 spot to the left blue arrow near $0\bar{1}$ peak and the distance from the 00 spot to the right blue arrow near 01 peak is $|\Delta\mathbf{k}_{\parallel}| = 2.36 \pm 0.05$ Å^{-1}. This value converts to real space in-plane lattice constant a = 3.07 ± 0.07 Å for ZnO(0001). Similarly, the average reciprocal space distance from 00 spot to the left red arrow near $0\bar{1}$ peak and the distance from the 00 spot to the right red arrow near 01peak is $|\Delta\mathbf{k}_{\parallel}| = 2.65 \pm 0.05$ Å^{-1}. This value converts to real space in-plane nearest neighbor distance $a_{nn} = 2.74 \pm 0.05$ Å for Au(111).

Similarly, a RHEED pattern in Fig. 10(c) at $\phi = 352.8^{o}$ that is 30^{o} azimuthal angle away from that at Fig. 10(a) was examined. Fig. 10(d) shows intensity *vs*. momentum transfer parallel to the surface $\mathbf{k}_{\parallel}$ integrated from the horizontal yellow box in Fig. 10(c). It shows similar paired double spots labelled as blue and red arrows at $\bar{1}2$, 00, and $1\bar{2}$ stripes. The average reciprocal space distance from 00 stripe to the right and left blue arrows and red arrows are $|\Delta\mathbf{k}_{\parallel}| = 4.00 \pm 0.10$ Å^{-1} and $|\Delta\mathbf{k}_{\parallel}| = 4.50 \pm 0.10$ Å^{-1}, respectively. These convert to real space in-plane lattice constant a = 3.14 ± 0.08 Å for ZnO(0001) and $a_{nn} = 2.79 \pm 0.06$ Å for Au(111). These values are consistent with that determined from Fig. 10(b).

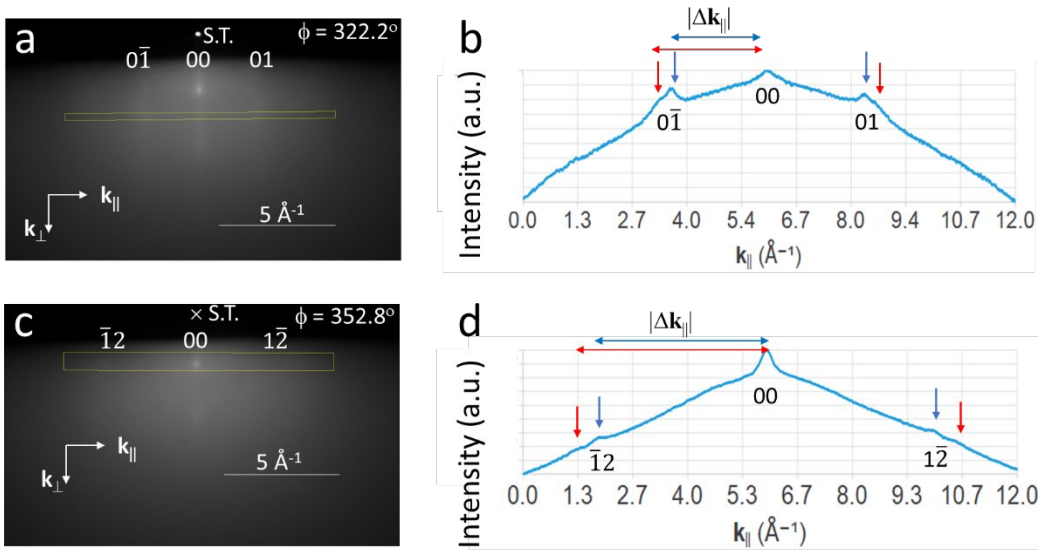

Fig. 10. (a) and (c) RHEED patterns of sample M (ZnO with 3.20% Au) viewed along the $[1\bar{2}10]$ and $[1\bar{1}00]$ zone axis directions, respectively. (b) and (d) Intensity *vs*. momentum transfer parallel to the surface $\mathbf{k}_{\parallel}$ from the horizontal yellow box in (a) and (c), respectively.

3.4.3.1.2 *Out-of-plane lattice constant from* $\Delta\mathbf{k}_\perp$

Figure 11(a) shows the same RHEED pattern at $\phi = 322.2^o$ as in Fig. 10(a). A visible spot near the center of a pattern and below the straight through (S.T.) spot is always seen in all patterns. This implies the spot is from transmission of glancing incident electron beam through surface features. Fig. 11(b) shows intensity *vs*. momentum transfer perpendicular to the surface $\mathbf{k}_\perp$ integrated from the vertical yellow box in Fig. 11(a). The vertical reciprocal spacing from S.T. beam at $\mathbf{k}_\perp = 0$ Å^{-1} to the visible spot below the S.T. spot labeled as a red arrow is ~2.40 Å^{-1}. This reciprocal spacing corresponds to 002 spot of ZnO. There is another much weaker intensity peak labeled as a 2nd red arrow on the background intensity at ~ 4.8 Å^{-1} from the S.T. spot. The average $\Delta\mathbf{k}_\perp$ from adjacent two spots from many patterns in different azimuthal angles $|\Delta\mathbf{k}_\perp| = 2.59 \pm 0.10$ Å^{-1}. Through the reciprocal relationship $d(002) = 2\pi/\Delta\mathbf{k}_\perp$ the real space spacing is 2.42 ± 0.09 Å. The measured value within the uncertainty is consistent with the interlayer spacing 2.35 Å of Au(111).

If the intensity profile *vs*. $\mathbf{k}_\perp$ is scanned from the non-00 stripe, the lattice difference between ZnO and Au show up as separated stripes. The intensity profile *vs*. $\mathbf{k}_\perp$ along the yellow line of the inner 01 spot/stripe to the left side of 00 stripe in Fig. 11(c) is shown in Fig. 11(d). Four visible bumps with almost equal $|\Delta\mathbf{k}_\perp|$ spacing are seen and indicated as blue arrows. The average $|\Delta\mathbf{k}_\perp|$ between adjacent two bumps are 1.23 ± 0.04 Å^{-1}. This converts to a real space interlayer spacing of 5.11 ± 0.17 Å through $2\pi/|\Delta\mathbf{k}_\perp|$, close to ZnO's bulk lattice constant c of 5.20 Å.

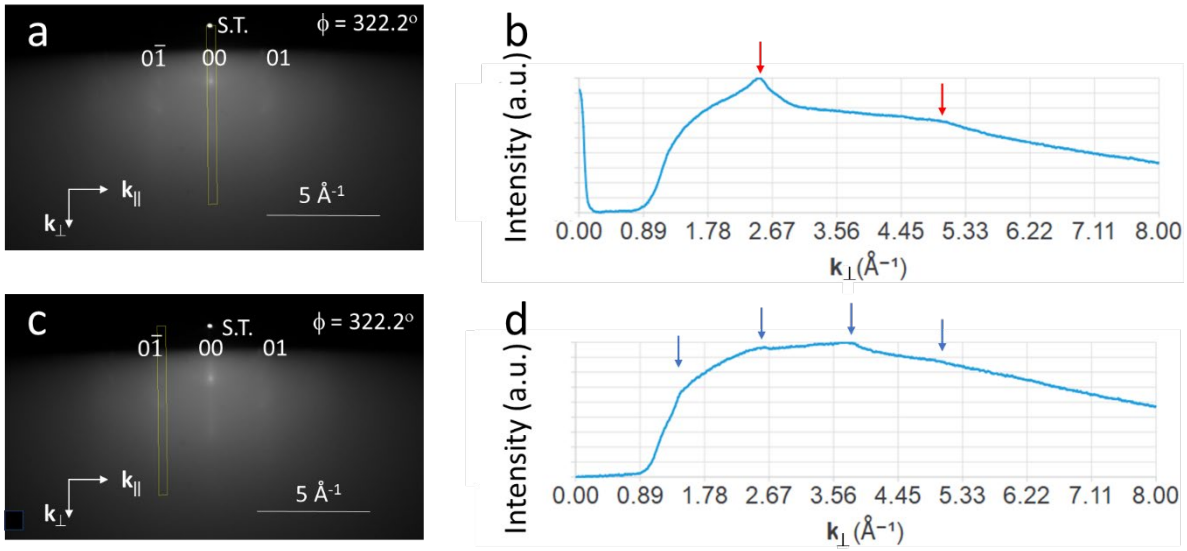

Fig. 11. (a) and (c) are the same RHEED pattern of sample M (ZnO with 3.2% Au) viewed along the [1$\bar{2}$10] zone axis direction. (b) and (d) Intensity *vs*. momentum transfer perpendicular to the surface $\mathbf{k}_\perp$ from the 00 stripe/spots and 0$\bar{1}$ stripe/spots along the vertical yellow box in (a) and (c), respectively.

3.4.3.2 2D map reveals pairs of double spots from ZnO and Au

Figure 12 shows a 2D reciprocal space map of ZnO with 3.20% Au constructed from azimuthal angle dependent RHEED patterns. Since the visible spot 002 in all patterns is located at $|\mathbf{k}_\perp| \sim 2.4$ Å^{-1}, we chose to present the 2D map parallel to the surface at the value of $|\mathbf{k}_\perp| = 2.34$ Å^{-1}. Among the 1st order diffraction only two spots at $\mathbf{k}_\parallel$ distance ~ 2.5 Å^{-1} can be clearly located. We label them 01 and $1\bar{1}$ from 012 and $1\bar{1}2$ spots by dropping the last index $l = 2$. The 2nd order diffraction has 4 obvious pairs of double spots near azimuthal angles 30^o, 150^o, 270^o, and 330^o at $\mathbf{k}_\parallel$ distance ~ 4 Å^{-1} and ~ 4.6 Å^{-1} from the center of the 2D map and indicated by 4 elongated circles. The spots near azimuthal angles 90^o and 210^o have weaker intensity. Despite the weak spots they are consistent with a 6-fold symmetry. Based on a simulated reciprocal space lattice from a hexagonal lattice one can assign the 4 spots counterclockwise as 11, $\bar{1}2$, $\bar{2}1$, $1\bar{2}$, and the 2 weaker spots as $\bar{1}\bar{1}$ and $2\bar{1}$.

The spots closer to the center in the pair of double spots have an average $|\Delta\mathbf{k}_\parallel| = \mathbf{G}(\bar{1}2) = 3.90 \pm 0.10$ Å^{-1} from patterns examined near the symmetrical directions. Where **G** is reciprocal space vector. Use the reciprocal relationship $\mathbf{G}(\bar{1}2) = 2\pi/d(\bar{1}2)$ and $d(\bar{1}2) = |\mathbf{a}|/2$, one obtains $|\mathbf{a}|_{ZnO} = 2\pi/(|\Delta\mathbf{k}_\parallel|/2) = 3.22 \pm 0.08$ Å. This value is consistent with bulk ZnO lattice constant a = 3.25 Å within experimental uncertainty.

Next, we analyze the spot further away from the center in the pair of double spots. Recall XRD θ *vs*. 2θ scan reveals the Au out-of-plane orientation is 111. For Au(111) out-of-plane orientation, the nearest neighbor distance in the lattice plane of Au(111) is 2.88 Å and the angle between two adjacent directions of two nearest neighbor distances is 60^o. The spots further away from the center in the pair of double spots have an average $|\Delta\mathbf{k}_\parallel| = \mathbf{G}(\bar{1}2) = 4.50 \pm 0.10$ Å^{-1} obtained from patterns near the symmetrical directions. Following the similar reciprocal relationship above, $|\mathbf{a}|_{Au} = 2\pi/(|\Delta\mathbf{k}_\parallel|/2) = 2.79 \pm 0.06$ Å. This value is slightly smaller than bulk Au's nearest neighbor distance, 2.88 Å. The experimentally measured lattice mismatch between Au and ZnO is 13 ± 2 % ($a_{ZnO} = 3.22 \pm 0.08$ Å and $a_{Au} = 2.79 \pm 0.06$ Å).

The 2D map of ZnO with 3.20% Au reveals a parallel epitaxy between Au(111) and ZnO(0001) because the two spots in each pair of double spots are radially parallel along 4 out of 6 major symmetric directions despite a 11.4% lattice difference between theoretical a = 3.25 Å for ZnO and nearest neighbor distance 2.88 Å for Au. However, compare the map with that of sample L, less number of the first order diffraction spots appear and the background is high around some hk spots indicating the epitaxy quality of sample M is less than that of sample L. TEM data from the next section will reveal more difference between samples L and M in small areas.

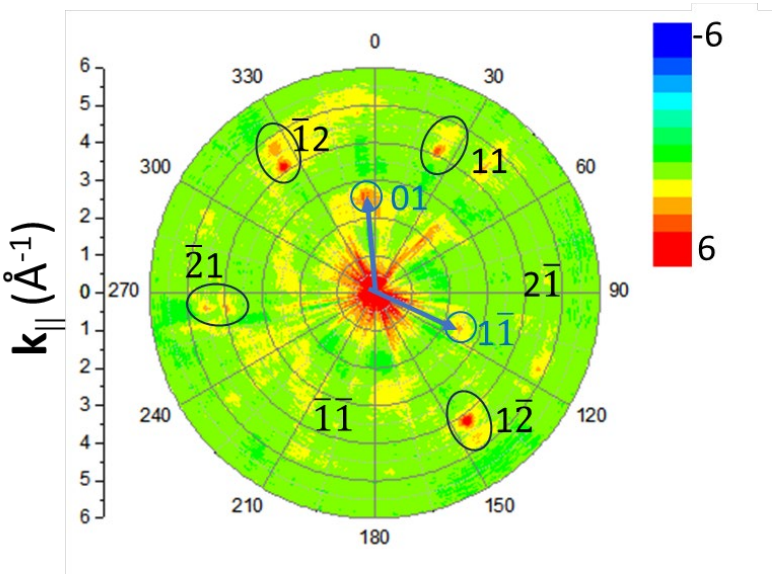

Fig. 12. A 2D reciprocal space map of sample M (ZnO with 3.20% Au) constructed from azimuthal angle dependent RHEED patterns. The unit vectors **a*** and **b*** with 60^{o} between two vectors are labeled. The map shows a 6-fold symmetry and doublet spots in circles that contains inner spot of ZnO and out spot of Au along the major symmetric directions.

3.5 TEM images and EDS maps of samples P, L, and M

Besides the structure imaged by TEM and elemental distribution maps of ZnO and Au obtained by EDS, the thicknesses of samples P, L, and M have been estimated from TEM cross section images in sections 3.5.1, 3.5.2, and 3.5.3 to be 15 ± 2 nm, 74 ± 2 nm, and 37 ± 2 nm, respectively.

3.5.1 TEM image and EDS map of ZnO on sapphire(0001)

Figure 13(a) shows a cross-section TEM image of ZnO on sapphire. Cr and Pt films were coated on ZnO before the FIB milling. TEM shows sharp diffraction peaks from substrate sapphire (not shown here) but no obvious diffraction spots from ZnO are observed implying amorphous or very small nanocrystalline ZnO. This is in contrast to stripes and spots observed in RHEED patterns in Fig. 4 and diffraction spots observed in the ARHEED 2D map in Fig. 5. This may be because 20 keV glancing incident electrons used in RHEED have short mean free path and can only probe near surface structure. As the ZnO film grows thicker, the initial small nanocrystals grow larger and the reflected high-energy electrons scatter from these larger crystals near surface of film contribute to the diffraction spots and stripes. Fig. 13(b) shows an EDS map of ZnO with Zn in red color. The thickness of ZnO estimated from Figs. 13(a) and 13(b) is about 15 ± 2 nm.

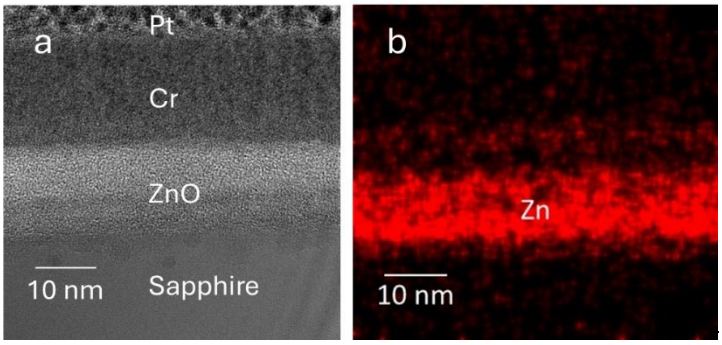

Fig. 13. Sample P (ZnO on sapphire). (a) Cross section TEM image showing ZnO on sapphire with Cr and Pt coatings on top of ZnO and sapphire substrate on the bottom. (b) EDS map of ZnO showing Zn in red.

3.5.2 TEM image and EDS map of sample L (ZnO with 1.95% Au) on sapphire

Figure 14(a) shows) high angle annular dark field (HAADF) image of sample L. The thickness of the film is 74 ± 2 nm. It shows dense column like features perpendicular to the sapphire substrate. The HADDF collects incoherently scattered electrons from nucleus of atoms and its contrast is proportional to atomic number Z^2. For higher Z, the image shows brighter signals. The Z numbers of Au and Zn are 79 and 30, respectively. Fig. 14(b), (c), and (d) show EDS elemental maps of Zn, Au, and combined Zn and Au, respectively. The contrast in EDS is proportional to the amount of element. The Zn distribution in red color is more uniform and continuous in Fig. 14(b) as compared with less uniform distribution of Au in green color in Fig. 14(c). Although there is 1.95% Au determined by XRD EDS, the Au nanoparticle distribution is over the entire thickness of the film implying that it functioning as a catalyst to assist the growth of a continuous ZnO film.

Figure 14(e) shows a high-resolution TEM cross section image of sample L. The sapphire crystal substrate at the bottom has a regular lattice with rectangular unit mesh. The scale bar is 2 nm. The film above sapphire substrate also has a regular lattice. A magnified image with a scale bar of 5 Å in the inset shows a rectangular mesh with lengths **c** (vertical) and $(\sqrt{3}/2)\mathbf{a_p}$ (subscript p means parallel to substrate surface). The measured c = 5.2 ± 0.2 Å and a_p = 2.8 ± 0.1 Å. Note $(\sqrt{3}/2)a = a_p$ and a = 3.2 ± 0.1 Å that is close to the lattice constant 3.25 Å of ZnO. The ratio of $|\mathbf{c}/\mathbf{a_p}|$ = 1.83 ± 0.03. A fast Fourier transform (FFT) of the ZnO ultrathin film in Fig. 14(e) is shown in Fig. 14(f). The reciprocal space mesh lengths are **c*** and $\mathbf{a_p}^*$ has a rectangular shape and rotates 90° relative to the real space unit mesh in Fig. 14(e). The ratio of $|\mathbf{a_p}^*/\mathbf{c}^*|$ = 1.83 ± 0.03, also consistent with $|\mathbf{c}/\mathbf{a_p}|$ in Fig. 14(e). This is consistent with the symmetry of diffraction pattern viewing zone direction along the [11$\bar{2}$0] direction.

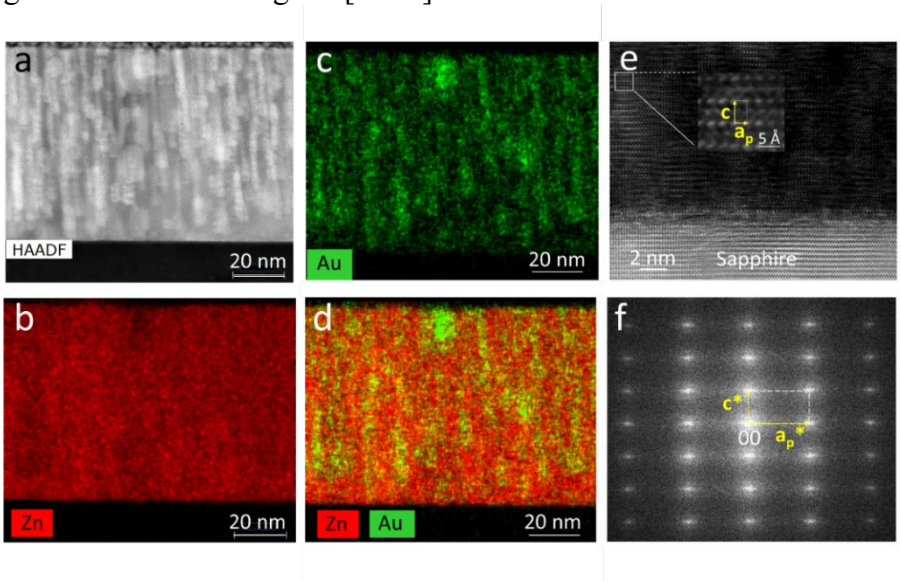

Fig. 14. Sample L (ZnO with 1.95% Au). (a) High angle annular dark field (HAADF) image. EDS maps of (b) Zn in ZnO, (c) Au, (d) combined Zn in ZnO and Au. (e) High-resolution cross section image of sample L, inset shows a rectangular mesh with lengths c and a_p. (f) Fast Fourier transform of ZnO with Au in the upper part of Fig. (e). A rectangular mesh with reciprocal space lengths c* and a_p^*.

3.5.3 TEM image and EDS map of sample M (ZnO with 3.20% Au) on sapphire

Figure 15(a) shows a cross-section TEM HAADF image of sample M. The thickness of the sample M is about 37 ± 2 nm. Intertwined nanoscale crystals with gaps are seen. It is less dense than sample L shown in Fig. 14(a). Figs. 15(b) and 15(c) show EDS map of Zn in red color from ZnO and EDS map of Au in green color, respectively. The intensity contrast of Zn and Au in the EDS maps of sample M are less uniform as compared with EDS maps in Figs. 14(b) and 14(c) from sample L. Fig. 15(d) is a combined EDS map of Zn and Au. Comparing the Au intensity from ZnO with 3.20% Au in Fig. 15(d) with that from ZnO with 1.95% Au in Fig. 14(d), the Au's contrast intensity is higher due to higher percentage of Au in sample M.

Fig. 15(e) shows a high-resolution TEM cross section image of ZnO. Certain planes and fringes are observed. A fast Fourier transform (FFT) of the yellow rectangular area in Fig. 15(e) is shown in Fig. 15(f) and this FFT shows spots with a certain symmetry. FFT has been performed on other crystals in Fig. 15(e) and different symmetries of diffraction spots are seen. No major preferred orientation can be easily identified since the crystal planes may not face the TEM viewing zone axis for a major symmetric direction closely. The deviations of crystal orientations from the major crystal symmetrical direction contribute to some missing hk diffraction spots and high background in the 2D map of sample M shown in Fig. 12. That the crystal size of sample M is larger than that of sample L observed in TEM images is also consistent with AFM images shown in Figs. 3(f) and 3(f) where the surface protrusion size of sample M is larger than that of sample L.

The sizes of intertwined colored regions in EDS map in Fig. 15(d) are comparable to the nanoscale crystals in Fig. 15(a). At the interface of ultrathin film and sapphire the EDS map shows more red color implying the ZnO maybe more dominant near the interface. If we assume that the Au nanocrystal is on top of ZnO nanocrystal, in the supplementary document a superlattice area matching simulation indicates a parallel epitaxy relationship between Au(111) and Zn(0001). The parallel epitaxy is consistent with the finding from samples L (ZnO with 1.95% Au) and sample M (ZnO with 3.20% Au).

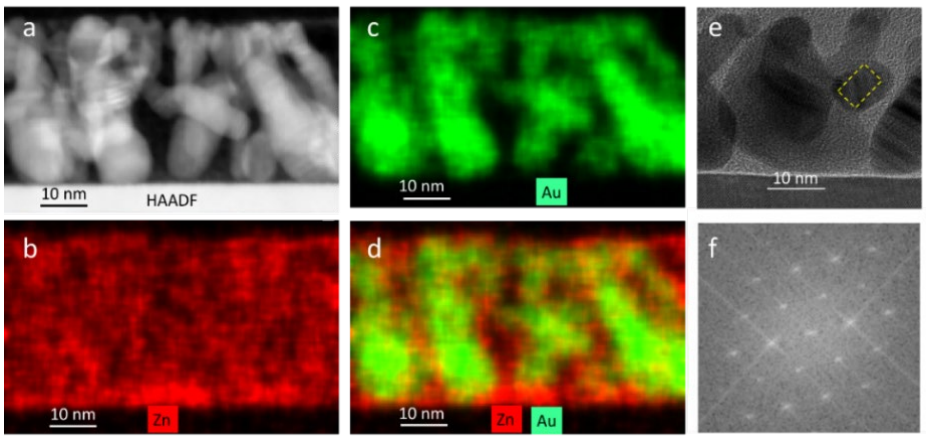

Fig. 15. Sample M (ZnO with 3.20% Au). (a) HAADF image. EDS maps of (b) Zn in ZnO, (c) Au, (d) combined Zn in ZnO and Au. (e) High-resolution cross section image, (f) Fast Fourier transform of dashed rectangular area in (e). Scale bars are 10 nm in (a) to (e).

4. Conclusion

PLD of ultrathin films of ZnO, ZnO with 1.95% atomic percent of Au, and ZnO with 3.20% atomic percent Au were grown on sapphire(0001) substrates by using single ZnO target with either a narrow or a wide Au stripe attached on the ZnO target. Surface and bulk sensitive techniques were used to characterize these films. The AFM images of ZnO, ZnO with 1.95% Au, and ZnO with 3.20% Au show continuous surface morphology on sapphire substrates with the vertical RMS values less than 0.2 nm. These ultrathin films are much smoother than past PLD grown ZnO film on sapphire reported in the literature.

For the near surface structures over a large area, the azimuthal dependent RHEED patterns of ZnO with 1.95% Au and ZnO with 3.20% Au show paired diffraction stripes/spots from ZnO(0001) and Au(111) along six-fold symmetrical directions due to 11.4% real space spacing difference. From the 2D reciprocal space map constructed from azimuthal RHEED patterns, they also show paired double spots. The out-of-plane orientations of ZnO and Au are ZnO(0001) and Au(111), respectively. The in-plane epitaxy relationships are Au$[\bar{1}10]$//ZnO$[2\bar{1}\bar{1}0]$ and Au$[\bar{1}01]$// ZnO$[11\bar{2}0]$ and both ZnO and Au have a 6-fold symmetry. RHEED and 2D map reveal ZnO and Au of sample L and M are epitaxy over a large area but are not able to distinguish whether ZnO and Au crystals form hetero-epitaxy laterally, vertically or a mixture.

Cross section TEM images and EDS maps were used to examine local area of sample L. TEM image and EDX map of ZnO with 1.95% Au reveal continuous ultrathin (74 ± 2 nm thick) ZnO nanocrystals with Au nanocrystals distribution over the continuous ultrathin ZnO film. FFT of high-resolution TEM image shows ZnO lattice but no Au lattice consistent with minute Au distribution in the EDS map. This supports the nanocluster Au with corners and edges serving as catalyst to promote the growth of ultrathin smooth epitaxial ZnO film. Note although the FFT of TEM does not show Au lattice, the ARHEED and 2D map over a large area show a strong ZnO lattice and a weaker Au lattice.

TEM image and EDS map of ZnO with 3.20% Au reveal less continuous but intertwined ZnO and Au nanocrystals with sizes larger than that in ZnO with 1.95% Au. Because TEM probes a small area, FFT of an individual crystal shows a crystalline symmetry but the crystal orientation among many crystals varies and is not easily identified as ZnO or Au. In contrast the ARHEED and 2D map over a large area show both ZnO lattice and Au lattice with some hk spots of ZnO or Au missing as well as a high background intensity over area between hk spots. Thus, the 2D map reveals the epitaxy quality of sample M is less than that of sample L.

In contrast RHEED patterns and 2D maps constructed from RHEED patterns of ZnO with 1.95% Au and ZnO with 3.20% reveal rich information including paired double spots, lattice constants determination, and epitaxy relationships over a large area. The complementary ARHEED, 2D maps, and TEM data support that a small atomic percentage of Au such as 1.95% can catalyze the growth of continuous epitaxial ultrathin films with sub nm RMS roughness. This study broadens the application of ARHEED on catalyst assisted growth of smooth epitaxial film by PLD.

CRediT authorship contribution statement

Xuegang Chen: Conceptualization, Funding acquisition, Supervision, Methodology, Validation
Guoliang Wang: Investigation, Formal analysis, Validation, Resources
Jijie Huang: Investigation, Formal analysis, Validation, Resources
Xurong Qiao: Investigation, Formal analysis, Validation, Resources
Zhen Zhang: Investigation, Formal analysis, Validation, Resources
Tao Li: Investigation, Formal analysis, Validation, Resources
Lihua Zhang: Investigation, Formal analysis, Validation, Writing - Review & Editing
Kim Kisslinger: Investigation, Formal analysis, Validation, Writing - Review & Editing
Zonghuan Lu: Writing - Review & Editing, Investigation, Formal analysis, Validation, Visualization
Neha Dhull: Investigation, Formal analysis, Validation
Weichang Lin: Investigation, Formal analysis, Validation
Toh-Ming Lu: Methodology, Writing - Review & Editing, Funding acquisition,
Gwo-Ching Wang: Conceptualization, Writing - Original Draft, Funding acquisition, Supervision, Methodology, Visualization

Acknowledgments
This work was supported by the Empire State Development's Division of Science, Technology and Innovation (NYSTAR) through Focus Center-New York contract C180117 and Rensselaer. We acknowledge Microscale and Nanoscale Cleanroom staff at RPI for in part facilitating the experimental work. This research used TEM at the Center for Functional Nanomaterials (CFN), which is a U.S. Department of Energy Office of Science User Facility, at Brookhaven National Laboratory under Contract No. DE-SC0012704. The work was also supported by the National Natural Science Foundation of China (Grants No. 12104005, Grant Nos. 52071258), the Scientific Research Foundation of the Higher Education Institutions for Distinguished Young Scholars in Anhui Province (Grants No. 2022AH020012), and the Innovation Project for Overseas Researcher in Anhui Province (Grants No. 2022LCX004). This work was also partially supported by the facilities at the Center of Free Electron Laser & High Magnetic Field (FEL & HMF) in Anhui University. We thank Chenyu Liang at Instrument Analysis Center of Xi'an Jiaotong University for assistance in XRD analysis.

Declaration of competing interest
The authors declare that they have no known competing financial interests or personal relationships that could have appeared to influence the work reported in this paper.

Supplementary materials
Supplementary material associated with this article can be found, in the online version, at….

Data availability
Data will be made available on request.

References

To be filled in from Wang's EndNote ref bank.

Supplementary document

Au assisted smooth ultrathin epitaxial ZnO film grown by pulsed laser deposition on sapphire(0001)

Xuegang Chen[1,2], Guoliang Wang[3], Jijie Huang[3], Xurong Qiao[4], Zhen Zhang[4], Tao Li[4], Lihua Zhang[5], Kim Kisslinger[5], Zonghuan Lu[6,7], Neha Dhull[6,7], Weichang Lin[6,7], Toh-Ming Lu[6,7], and Gwo-Ching Wang[6,7]

[1] Center of Free Electron Laser & High Magnetic Field, Institutes of Physical Science and Information Technology, Anhui University, Hefei 230601, China
[2] Information Materials and Intelligent Sensing Laboratory of Anhui Province, Anhui Key Laboratory of Magnetic Functional Materials and Devices, Anhui University, Hefei 230601, China
[3] School of Materials, Shenzhen Campus of Sun Yat-sen University, Shenzhen 518107, China
[4] State Key Laboratory for Mechanical Behavior of Materials, Department of Materials Science and Engineering, Xi'an Jiaotong University, Xi'an, Shaanxi 710049, China
[5]Brookhaven National Laboratory, Center for Functional Nanomaterials, P.O. Box 5000, Upton, New York 11973, USA
[6]Physics, Applied Physics and Astronomy Department, Rensselaer Polytechnic Institute, Troy, NY 12180, USA
[7]Center for Materials, Devices and Integrated Systems, Rensselaer Polytechnic Institute, Troy, NY 12180, USA

Corresponding authors: Gwo-Ching Wang wangg@rpi.edu; Xuegang Chen xgchen@ahu.edu.cn

S1. In-plane epitaxial relationship between ZnO and substrate Al_2O_3 measured by XRD azimuthal scans

Based on the out-of-plane orientation determined from XRD θ *vs*. 2θ scan of ZnO(0001) on sapphire(0001), one can use azimuthal scan of an X-ray pole to determine its in-plane epitaxial relationship. Figs. S1(a)-(d) show the azimuthal scans of poles: ZnO{$10\bar{1}2$}, ZnO{$11\bar{2}2$}, sapphire {$10\bar{1}2$}and sapphire {$11\bar{2}3$}. The ZnO{$10\bar{1}2$}, ZnO{$11\bar{2}2$}, and sapphire {$11\bar{2}3$} scans show 6 peaks. The sapphire {$10\bar{1}2$} scan shows 3 peaks consistent with trigonal (Rhombohedral) lattice symmetry. Simulated pole figures of ZnO(0001) and Al_2O_3(0001) are shown in Figs. S1(e) and S1(f), respectively. Note the simulated ($11\bar{2}0$) for both ZnO and Al_2O_3 are aligned. However, experimental observation is that ($11\bar{2}0$) for ZnO and ($11\bar{2}0$) for Al_2O_3 has a 30° relative in-plane rotation. In other words, if the simulated pole figure ZnO(0001) rotates in-plane by 30° from the original simulated pole figure, then it consistent with experimental Φ scan of {$11\bar{2}0$} poles. The experimentally determined epitaxial relationships are in-plane ZnO($10\bar{1}0$)//sapphire($11\bar{2}0$) and ZnO($11\bar{2}0$)//sapphire($10\bar{1}0$). We conclude the ZnO and sapphire have a 30° in-plane rotation relative to each other.

Due to the low photo counts in XRD intensity of Au(111) peak, the azimuthal scan of an Au pole figure was not performed and the relative epitaxy relationship between Au and ZnO cannot be determined by XRD azimuthal scan. However, one can use 2D map constructed from azimuthal reflection high energy electron diffraction (ARHEED) patterns to determine the epitaxial relationship presented in the main text for ZnO with 1.95% Au and for ZnO with 3.20% Au because the scattering intensity of electrons is four orders of magnitude higher than that of X-ray photons.

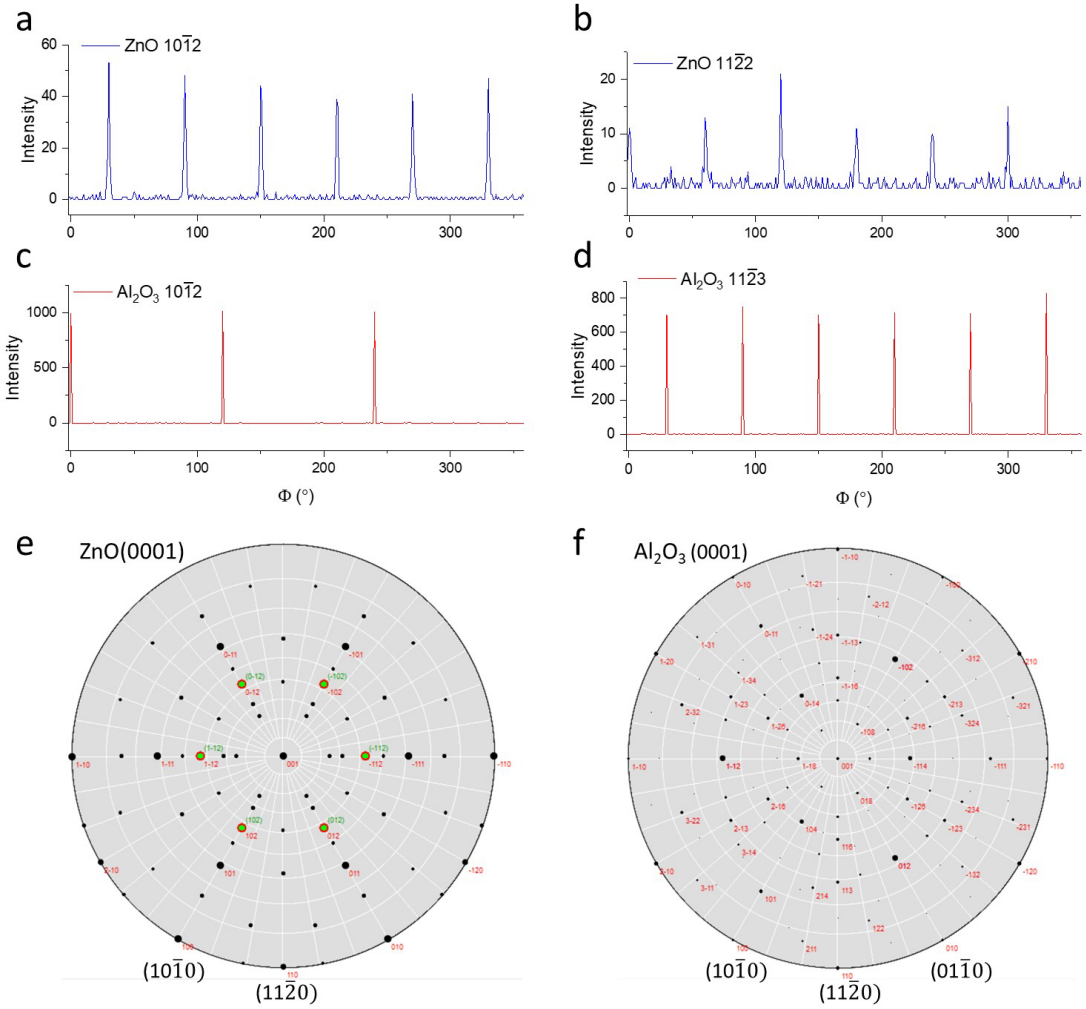

Fig. S1 X-ray azimuthal scans of poles. (a) ZnO{10$\bar{1}$2}, (b) ZnO{11$\bar{2}$2}, (c) sapphire {10$\bar{1}$2}and (d) sapphire {11$\bar{2}$3}. Both experimental ZnO{10$\bar{1}$2} and ZnO{11$\bar{2}$2} poles have a relative 30^o in-plane rotation with respect to sapphire {10$\bar{1}$2} and sapphire {11$\bar{2}$3} poles. (e) WinWulff simulations of pole figures ZnO(0001) and (f) Sapphire(0001). ZnO{10$\bar{1}$2} poles are 0^o rotated from sapphire {10$\bar{1}$2} poles and so are ZnO{11$\bar{2}$2} poles relative to sapphire {10$\bar{1}$2} poles. The simulated poles of ZnO should rotate 30^o in-plane to match experimental observed 30^o rotation.

S2. In-plane symmetry of ZnO film measured by EBSD

EBSD pole figures, inverse pole figure in the Z direction normal to sample surface (IPF-Z), and IPF maps of samples R, L, and M are shown in Figs. S2(a), S2(b), and S2(c), respectively. No sapphire is detected from all three samples implying the ZnO is thicker than the penetration depth of electrons used in EBSD and electrons cannot reach the sapphire substrate. The (0001) pole figures have one pole, both $\{10\bar{1}2\}$ and $\{11\bar{2}3\}$ pole figures have 6 poles in each. The IPF-Z and IPF-X maps (in sample's Z and X directions) of ZnO show uniform color over 50 μm × 40 μm area indicating single crystal ZnO. The pole figures and IPF of ZnO with 1.95% Au and ZnO with 3.20% Au are similar to that of ZnO. However, the IPF maps of ZnO with 1.95% Au and ZnO with 3.20% Au have some black spots that are dead resolution areas (probably could be due to surface contamination or roughness, or Au nanocrystals). The number of black spots in ZnO with 1.95% Au is less than that of ZnO with 3.20% Au. The Kikuchi pattern of ZnO with 3.20% Au is also weaker than that of ZnO (not shown). This implies a slightly worse crystal quality of ZnO with 3.20% Au as compared with that of ZnO with 1.95% Au and without Au. This EBSD result from near surface regions of three samples are consistent with the result of ARHEED patterns and 2D maps from surfaces.

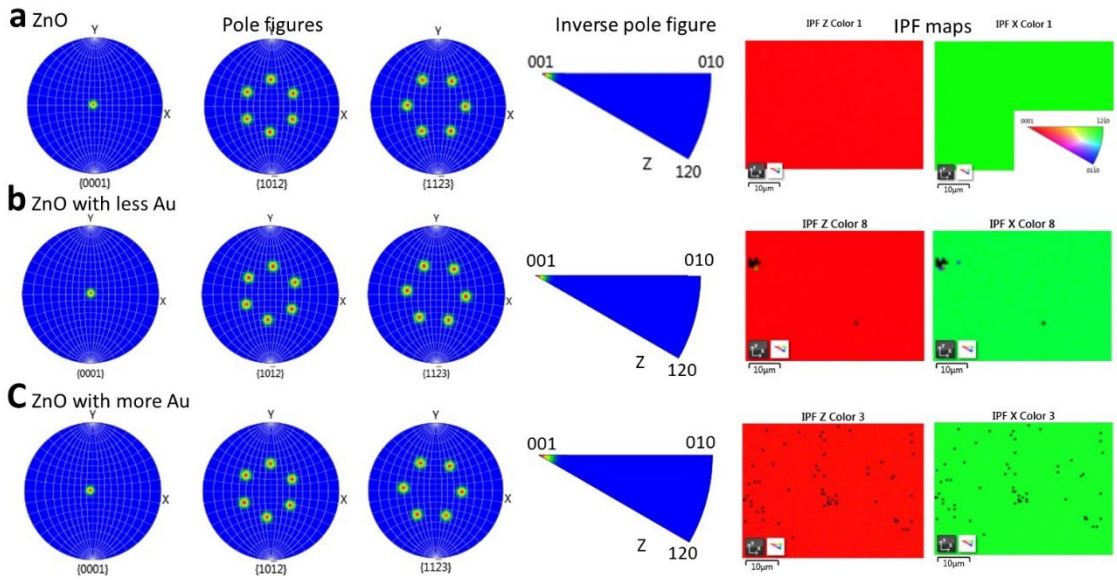

Fig. S2 EBSD pole figures, inverse pole figure in the Z direction normal to sample surface (IPF-Z), and IPF maps of (a) ZnO on sapphire, (b) ZnO with 1.95% Au, and (c) ZnO with 3.20% Au. The resolution of EBSD is not able to resolve paired double spots from ZnO and Au. In contrast the ARHEED patterns and 2D maps described in the main text can resolve the paired double spots.

S3. Geometrical superlattice area matching (GSAM) model for ZnO(0001) on sapphire(0001) and Au(111) on sapphire(0001)

As described in the main text, the epitaxy relationship of a heteroepitaxy system can be predicted by a geometrical superlattice area matching (GSAM) model [Yapsir, Al/Si, 1990; Zur 1984; Tokarský 2024]. A parameter called superlattice area mismatch, ΔA, is defined as follows: $\Delta A = A[(\Delta u/u) + (\Delta v/v) + (\Delta\alpha/\tan\alpha)]$. The sides (2D lattice) of substrate superlattice are defined as u_1 and v_1 with an angle α_1 between them. The sides of overlayer superlattice are defined as u_2 and v_2 with an angle α_2 between them. The superlattice mismatch is defined as $\Delta u \equiv u_2 - u_1$, $\Delta v \equiv v_2 - v_1$, and $\Delta\alpha \equiv \alpha_2 - \alpha_1$. A_1 and A_2 are the superlattice areas of the substrate and overlayer, respectively.

This model is applied to ZnO on sapphire (Al_2O_3). Fig. S3(a) shows a ball model of superposed ZnO lattice in grey color balls on Al_2O_3 lattice in blue color balls. The bottom of Fig. S3(a) indicates the unit vectors **a** and **b** for ZnO and Al_2O_3 along the $[2\bar{1}\bar{1}0]$ and $[\bar{1}2\bar{1}0]$ directions, respectively, with 120° between unit vectors. The unit vector lengths a_{ZnO} and $a_{Al_2O_3}$ are 3.25 Å and 4.76 Å, respectively. Right above the unit vectors are the corresponding unit meshes of ZnO and sapphire lattices parallel to the interface. Fig. S3(b) is a result of GSAM simulation with input parameters a_{ZnO} = 3.25 Å, $a_{Al_2O_3}$ = 4.76 Å, 120° angle between unit vectors, max area 50 nm^2, mismatch 0.19, and angle minimum 30°. The simulation shows a minimum area of ΔA at rotation angle γ of 30°, 90°, and every 60° beyond (not shown in the plot). The superlattice unit meshes of ZnO in gray and Al_2O_3 in blue are indicated in the upper right corner of Fig. S3(a). The superlattice unit mesh area of Al_2O_3's 19.62 $Å^2$ that is the same as the original Al_2O_3 unit mesh. The ZnO superlattice unit mesh length is 5.63 Å whereas the original unit mesh length is 3.25 Å. The ZnO superlattice area of 27.45 $Å^2$ is three times of the original ZnO unit mesh area of 9.15 $Å^2$. The relative angle between ZnO and Al_2O_3 superlattices is 30°. If the ZnO superlattice unit mesh is rotated 30° clockwise, the ZnO and Al_2O_3 will have most lattice sites overlap in superlattice areas as seen in Fig. S3(c). This is consistent with the XRD azimuthal angle ϕ scans that show a 30° rotation between ZnO and Al_2O_3 as well as the 6-fold symmetry.

Geometrical superlattice area matching prediction for Au(111) on sapphire(0001) is also simulated. The result predicts a 30° rotation between Au and Al_2O_3 similar to that in Fig. S3 and is not shown here. The same 30° rotation between Au and Al_2O_3 and between ZnO and Al_2O_3 means ZnO and Au epitaxial is parallel to each other and is observed in 2D map and presented in section 3.4.2 and 3.4.3 in the main text.

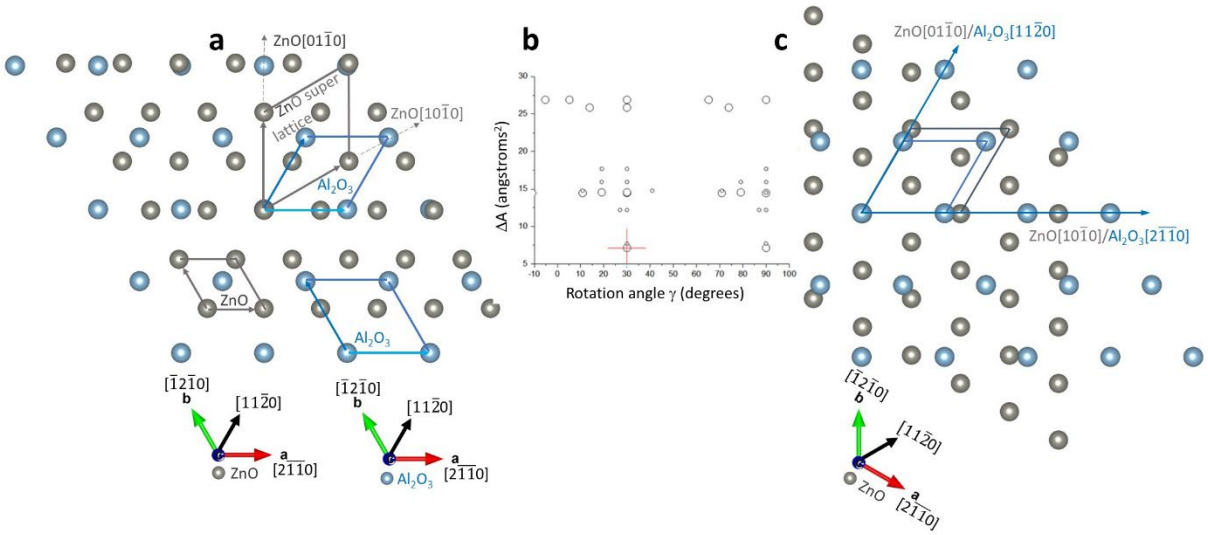

Fig. S3 (a) Ball models of 2D lattices for ZnO(0001) (grey color overlayer) on sapphire(0001) (blue color underlayer). Units meshes of ZnO(0001) and sapphire(0001) with angle between unit vector are sketched near the bottom. The directions are labeled. (b) Simulated geometrical superlattice area matching, ΔA plot for ZnO and sapphire. The rotation angle γ is defined as the angle between superlattices ZnO and sapphire. The minimum ΔA is the best superlattice matching. The radius of the circles in is inversely proportional to ΔA value. (c) When ΔA is minimum, the γ is 30°, the configuration predicted in (b), the superlattice of ZnO direction' [01$\bar{1}$0] rotates 30° in (a) and aligns with sapphire in the sketched. The sketched superlattice unit meshes before 30° rotation are sketched in the upper part of (a).

S4. Geometrical superlattice area matching (GSAM) model of Au(111) on Zn(0001) showing parallel epitaxy

TEM elemental map shows at the interface there are ZnO on the substrate sapphire and Au is on ZnO. To find out the relative epitaxy orientation between Au(111) lattice and ZnO(0001) lattice, a geometrical superlattice area matching (GSAM) model was used [Yapsir, Al/Si 1990; Zur 1984; Tokarský 2024]. A parameter called superlattice area mismatch, ΔA, is defined in section S3. Fig. S4(a) shows the calculated possible ΔA using lattice constants of a_{Au} = 2.88 Å and a_{ZnO} = 3.25 Å. The rotation angle is defined as the angle between $\mathbf{a}_{Au}$ and $\mathbf{a}_{ZnO}$. The maximums of A, Δu/u, Δv/v, and Δα/tanα are set to be 20 Å^2, 3%, 3%, and 3%, respectively. The radius of the circles in Fig. S4(a) is inversely proportional to ΔA. The smallest ΔA or the largest circles are at rotation angles 0^o or 60^o consistent with experimental observation.

Figure S4(b) shows real space lattices of ZnO and Au in grey and gold colors, respectively. The real space unit vectors **a**, **b** and **c** for cubic Au are shown as red, green, and blue arrows, respectively. The unit vector length a_{Au} of FCC Au is 4.078 Å. The nearest neighbor distance in the Au(111) plane is along the $[\bar{1}10]$ direction with length $a_{Au,nn} = a_{Au}/\sqrt{2}$ = 2.88 Å. The real space unit vectors **a** and **b** for hexagonal (0001) plane for ZnO are shown as red and green arrows, respectively. The **c** axis is perpendicular and out-of-the page. The unit vector length a_{ZnO} of ZnO is 3.25 Å along the $[2\bar{1}\bar{1}0]$ direction. The GSAM result indicates that Au's $[\bar{1}10]$ direction is parallel to the $[2\bar{1}\bar{1}0]$ direction of ZnO and Au's $[\bar{1}01]$ direction is parallel to the $[11\bar{2}0]$ direction of ZnO, a parallel epitaxy.

Due to the 11.4% lattice mismatch between $a_{Au,nn}$ = 2.88 Å and a_{ZnO} = 3.25 Å in real space, the reciprocal space vectors **G**(01) for Au and ZnO are $\mathbf{G}(01)_{Au} = \mathbf{a}^*_{Au,nn} = 2\pi/(2.88\sqrt{3}/2$ Å) = $2\pi/2.49$ Å = 2.52 Å^{-1} and $\mathbf{G}(01)_{ZnO} = \mathbf{a}^*_{ZnO} = 2\pi/(3.25\ \sqrt{3}/2$ Å) = $2\pi/(2.81$Å) = 2.23 Å^{-1}, respectively. The difference $\Delta(01) = \mathbf{G}(01)_{Au,nn} - \mathbf{G}(01)_{ZnO}$ =2.52 Å^{-1} – 2.23 Å^{-1} = 0.29 Å^{-1}. For Δ(02) = 2 × Δ(01) = 0.58 Å^{-1} and Δ(03) = 3 × Δ(01) = 0.87 Å^{-1}. This increasing reciprocal spacings separation as the order of diffraction increases are observed as 0.30 ± 0.05 Å^{-1}, 0.59 ± 0.05 Å^{-1}, and 0.92 ± 0.10 Å^{-1} in experimental intensity profile along **G**(01) direction in Fig. 4(b) in the main text. For $\mathbf{G}(11)_{ZnO} = 2\pi/(3.25/2$ Å) = $2\pi/(1.62$Å) = 3.86 Å^{-1}, and $\mathbf{G}(11)_{Au,nn}$ = $2\pi/(2.88/2$ Å) = $2\pi/(1.62$Å) = 4.36 Å^{-1}, the difference Δ(11) = 4.36 Å^{-1} – 3.86 Å^{-1} = 0.50 Å^{-1}. Experimentally we observed 0.54 ± 0.05 Å^{-1}, consistent with experimental results presented in Fig. 6(c) in the main text within experimental uncertainty.

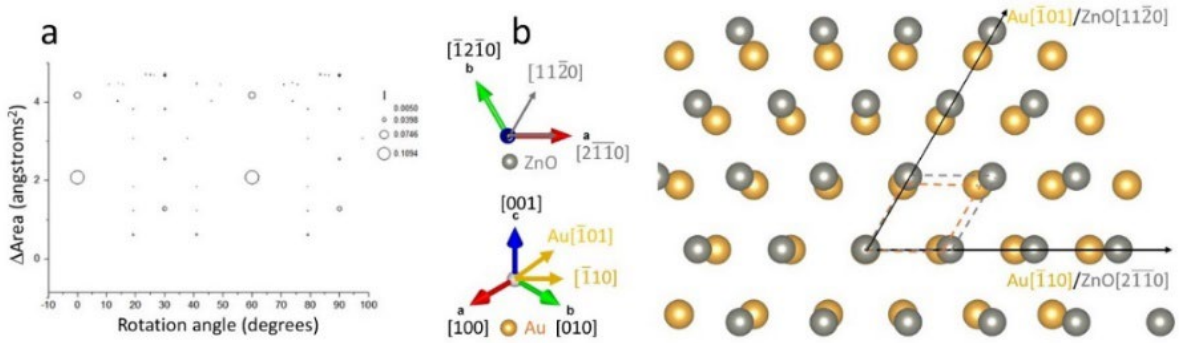

Fig. S4 Simulated geometrical superlattice area mismatching ΔA plot for ZnO and Au assuming Au is overlayer and ZnO is underlayer. The rotation angle γ is defined as the angle between superlattices $\mathbf{a}_{Au}$ and $\mathbf{a}_{ZnO}$. (b) 2D superlattices for Au(111) (orange color) on ZnO(0001) (grey color) when the γ is 0°, which is the most favorable configuration predicted in (a) as parallel epitaxy.